DOT/FAA/NR-90/6

Project Report
ATC-177

Beam Filling Loss Adjustments for ASR-9 Weather Channel Reflectivity Estimates

C. D. Engholm
S. W. Troxel

22 October 1990

Lincoln Laboratory
MASSACHUSETTS INSTITUTE OF TECHNOLOGY
LEXINGTON, MASSACHUSETTS

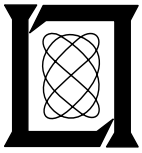

Prepared for the Federal Aviation Administration,
Washington, D.C. 20591

TECHNICAL REPORT STANDARD TITLE PAGE

1. Report No.	2. Government Accession No.	3. Recipient's Catalog No.
ATC-177	DOT/FAA/NR-90/6	

4. Title and Subtitle
Beam Filling Loss Adjustments for ASR-9 Weather Channel Reflectivity Estimates

5. Report Date
22 October 1990

6. Performing Organization Code

7. Author(s)
Cynthia D. Engholm and Seth W. Troxel

8. Performing Organization Report No.
ATC-177

9. Performing Organization Name and Address
Lincoln Laboratory, MIT
P.O. Box 73
Lexington, MA 02173-9108

10. Work Unit No. (TRAIS)

11. Contract or Grant No.
DTFA-01-L-83-4-10579

12. Type of Report and Period Covered
Project Report

12. Sponsoring Agency Name and Address
Department of Transportation
Federal Aviation Administration
Systems Research and Development Service
Washington, DC 20591

14. Sponsoring Agency Code

15. Supplementary Notes
This report is based on studies performed at Lincoln Laboratory, a center for research operated by Massachusetts Institute of Technology under Air Force Contract F19628-90-C-0002.

16. Abstract

The FAA is deploying over 100 new airport surveillance radars (ASR-9) across the country. In contrast to earlier ASRs, the ASR-9 utilizes a separate digital weather processing channel to provide air traffic controllers with timely, calibrated displays of precipitation intensity. The ASR-9 utilizes dual selectable fan-shaped elevation beams designed to track aircraft over a large volume. As a consequence, weather echoes received from these fan-shaped beams represent vertically-averaged quantities. If the precipitation only partially or non-uniformly fills the beam, then the vertically integrated reflectivity may underestimate the actual intensity of the storm. The ASR-9 weather channel corrects for this by adjusting the range-dependent six-level reflectivity thresholds. The appropriateness of the currently implemented correction has not been carefully examined and may require modification to take into account regional and morphological variability in storm structure.

This reports discusses the method used to derive new beam filling loss adjustments. An extensive database of volumetric pencil-beam radar data were used in conjunction with our ASR-9 simulation facility to derive adjustments aimed at calibrating the precipitation intensity reports to the maximum perceived hazard. Results from this calibration indicate that a single correction is appropriate for all sites and intensities. The new corrections yield substantially improved results over the current corrections in producing these reflectivity reports.

17. Key Words
airport surveillance radar
ASR-9
weather channel
fan-beam radar
pencil-beam radar
precipitation
reflectivity
vertical reflectivity profile
reflectivity estimate accuracy
beamfilling compensation
spatial smoothing
computer simulation
regional variability

18. Distribution Statement
Document is available to the public through the National Technical Information Service, Springfield, VA 22161.

19. Security Classif. (of this report)	20. Security Classif. (of this page)	21. No. of Pages	22. Price
Unclassified	Unclassified	60	

FORM DOT F 1700.7 (8-72) Reproduction of completed page authorized

ABSTRACT

The FAA is deploying over 100 new airport surveillance radars (ASR-9) across the country. In contrast to earlier ASRs, the ASR-9 utilizes a separate digital weather processing channel to provide air traffic controllers with timely, calibrated displays of precipitation intensity. The ASR-9 utilizes dual selectable fan-shaped elevation beams designed to track aircraft over a large volume. As a consequence, weather echoes received from these fan-shaped beams represent vertically-averaged quantities. If the precipitation only partially or non-uniformly fills the beam, then the vertically integrated reflectivity may underestimate the actual intensity of the storm. The ASR-9 weather channel corrects for this by adjusting the range-dependent six-level reflectivity thresholds. The appropriateness of the currently implemented correction has not been carefully examined and may require modification to take into account regional and morphological variability in storm structure.

This report discusses the method used to derive new beam filling loss adjustments. An extensive database of volumetric pencil-beam radar data were used in conjunction with our ASR-9 simulation facility to derive adjustments aimed at calibrating the precipitation intensity reports to the maximum perceived hazard. Results for this calibration indicate that a single correction is appropriate for all sites and intensities. The new corrections yield substantially improved results over the current corrections in producing these reflectivity reports.

ACKNOWLEDGMENTS

The authors would like to thank and commend Charlie Lebell, Paul Morin and Janice Williams for their invaluable assistance with the data processing. Thanks also to Cindy Meuse for her help with several of the figures.

TABLE OF CONTENTS

LIST OF ILLUSTRATIONS

LIST OF TABLES

1. INTRODUCTION

1.1. BEAM FILLING LOSS PROBLEM

The Federal Aviation Administration (FAA) is deploying a new airport surveillance radar, the ASR–9, at over 100 airports across the United States, with some units already in operation. Like previous ASRs, the ASR–9 utilizes dual, broad elevation fan beams (Figure 1) along with a rapid scan rate (12.5 RPM) to perform its primary function of detecting aircraft over a 60 nmi radius. In contrast to previous ASRs, however, the ASR–9 possesses a separate dedicated weather processing channel which provides air traffic controllers with quantitative reports of precipitation intensity on their PPI displays. The ASR–9 weather channel reports are quantized according to the six levels used by the National Weather Service (NWS) and are related to radar weather reflectivity factor (dBZ) as shown in Figure 2.

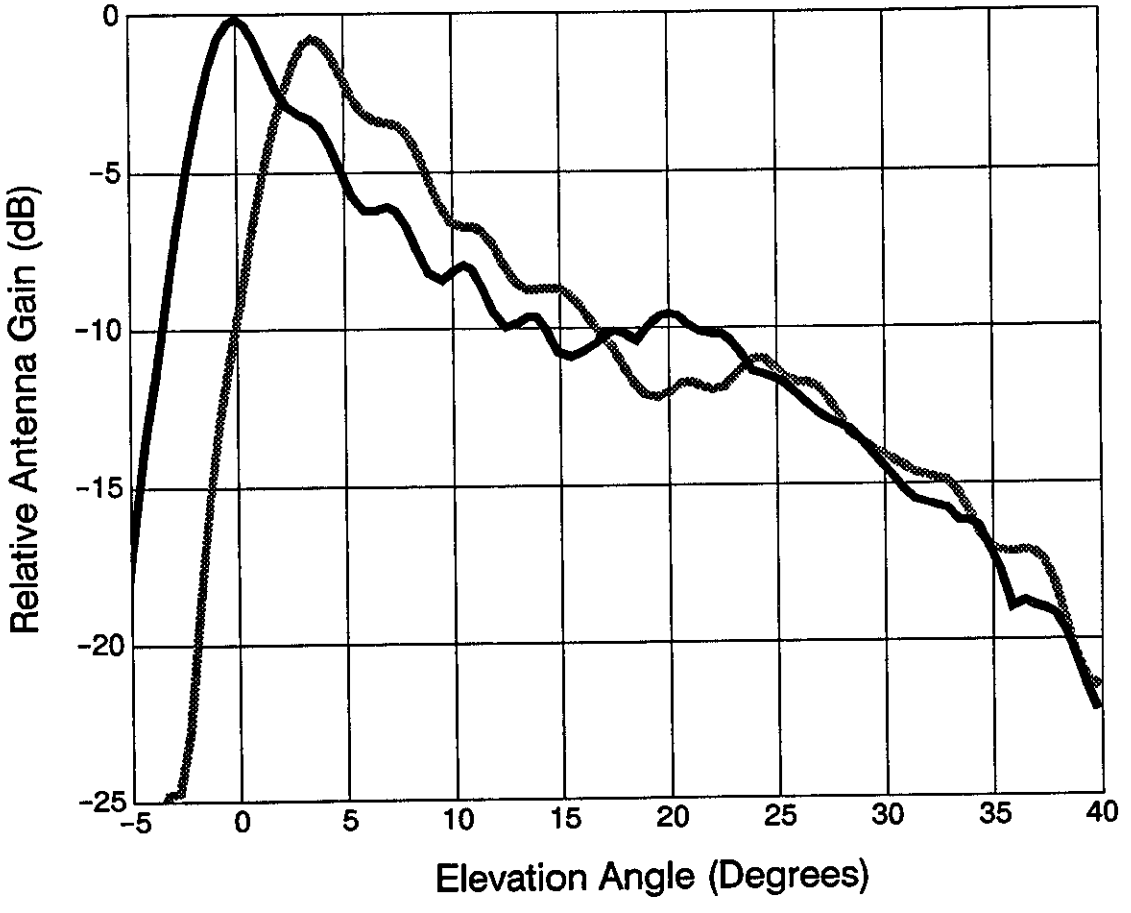

Figure 1. ASR–9 antenna pattern in the principal elevation plane. The low beam is plotted with a black curve and the high beam is plotted with a gray curve. The antenna is assumed to be positioned parallel to the horizon.

Although many features of the ASR–9, such as pulse repetition frequency (PRF), transmitter frequency, and pulse width, make it suitable for weather sensing, the broad elevation (4.8°) beams present a challenge for accurate determination of storm intensity. The PPI

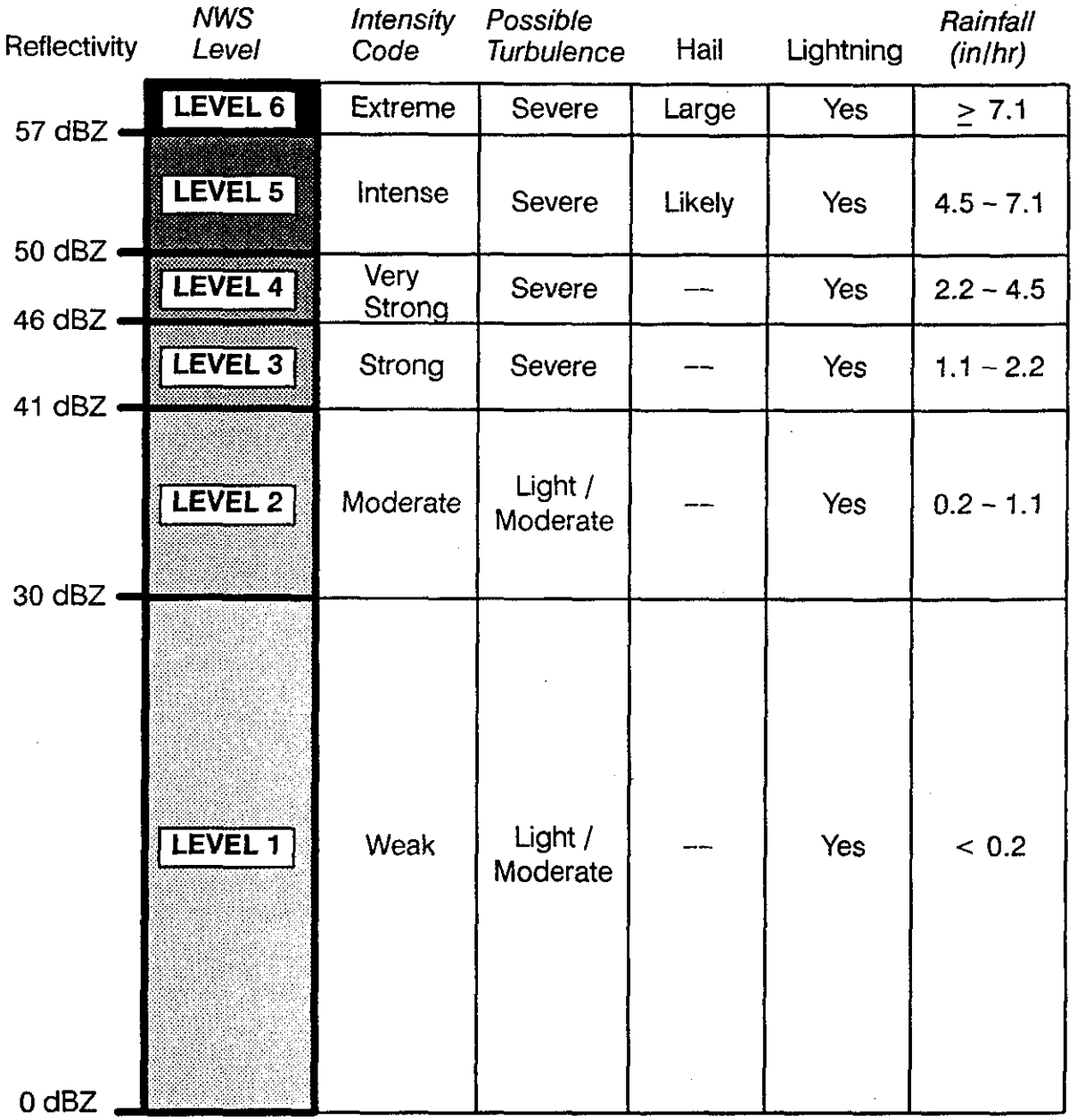

Figure 2. NWS standard reflectivity levels and associated weather.

weather display should provide the controller with a representative picture of the storm conditions likely to be encountered by an aircraft. Since the antenna gain varies with elevation angle (Figure 1), the parameter reported by the weather channel represents a beam-weighted, vertically averaged estimate of storm intensity. If the beam is non-uniformly or only partially filled with precipitation, then the inherent vertical integration introduced by the fan beam may cause an underestimate of the intensity of the storm. This beam filling loss (Figure 3) is most acute at long range, where the vertical extent of the beam intercepts more than 30,000 ft (9 km) of altitude. At short range, the fixed elevation scan is most sensitive to precipitation in the lower portion of the storm. The magnitude of the beam filling loss depends on the complex relationship between the vertical reflectivity structure of the storm and its interception by the fan-shaped beam. If the shape and altitude extent of the storm

vertical reflectivity profile (such as could be provided by a scanning pencil-beam radar) are known, then a suitable adjustment can be calculated and applied to the fan beam reflectivity estimate in order to produce the desired reflectivity report.

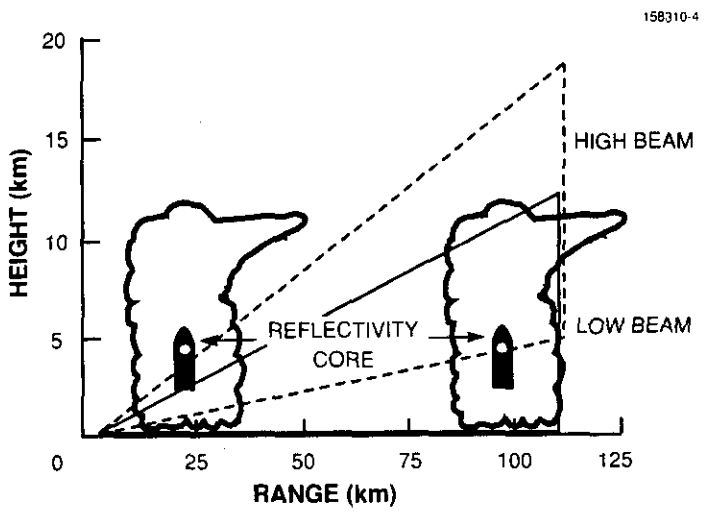

Figure 3. Schematic illustration of ASR-9 beam filling problem. Altitude limits of the -3 dB points on the ASR-9 antenna pattern are shown for the high (dashed) and low (solid) beam. A 2.0° antenna tilt is assumed.

Many parameterizations of the vertical reflectivity profile are possible. The purpose of the parameterization is to represent storm hazard. The most conservative report is the maximum reflectivity at any altitude. It is sensitive to regions of strong intensity regardless of their vertical extent. From a safety viewpoint, it is always desirable to avoid regions of high reflectivity, thus the vertical maximum reflectivity may be appropriate operationally. For this reason, the vertical maximum reflectivity will be the desired parameterization used in this report.

Several studies conducted in the 1960's and 1970's examined vertical reflectivity profiles. Donaldson (1961) studied 233 profiles from the cores of New England thunderstorms with maximum reflectivity greater than 50 dBZ. He classified the profiles into four groups: rain, hail, $\geq 1/2''$ hail, and tornado. He then computed the median profile from each profile group. 182 (78 percent) of the profiles were "rain" profiles, and their median profile shows maximum reflectivity at the surface and decreasing reflectivity with height, as shown in Figure 4 (open circle profile). In the other three categories, he found that the maximum reflectivity region in the median profile was elevated, with the elevated region centered around 20,000 ft (6 km) (see solid, dashed, and dotted profiles in Figure 4). These more severe median profiles are similar to what would be obtained by taking a profile through the core of the clouds depicted in Figure 3.

In another study, Konrad (1978) examined over 800 vertical reflectivity profiles taken through storm cores at a variety of locations. He grouped the profiles into 5 dBZ bins from 35 to 70 dBZ and found that mean profiles (Figure 5) from different locations were similar in shape but varied in the altitude extent of profile features, such as the depth of the maximum

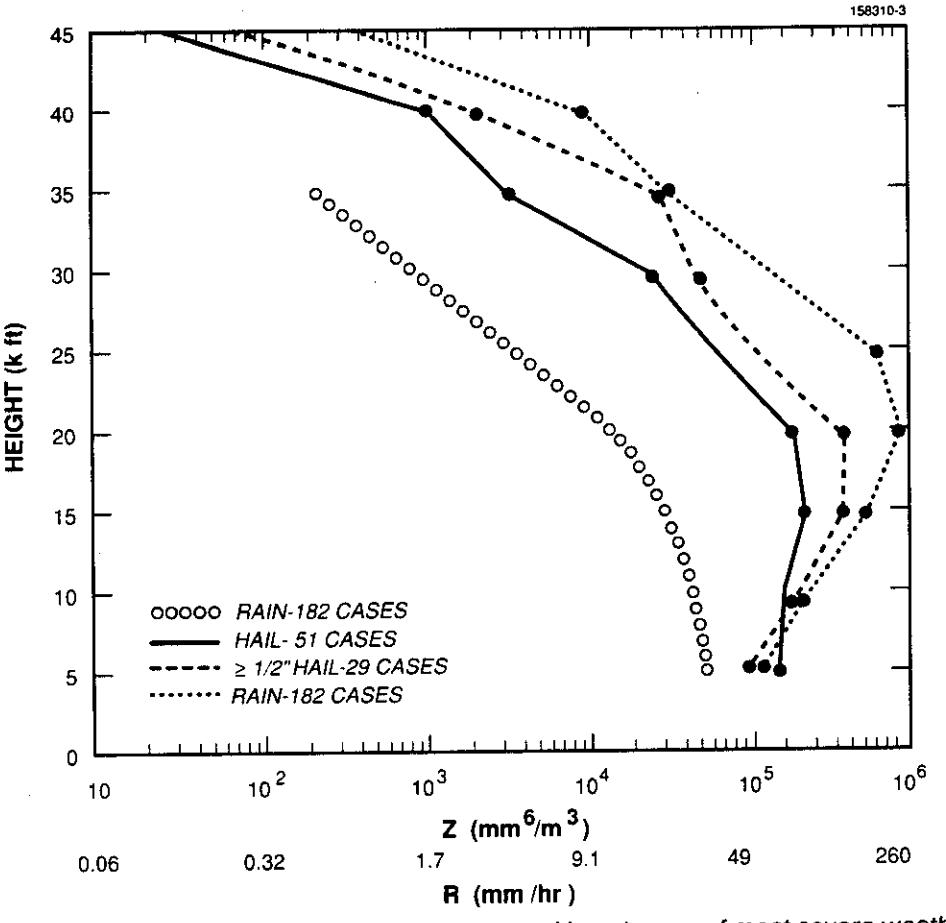

Figure 4. Median profiles of core reflectivity arranged in category of most severe weather. The 51 cases of hail include the 29 cases of large hail which are plotted separately. The 11 tornadic profiles are taken from the all-inclusive rain and hail categories. (After Donaldson, 1961.)

reflectivity region. He found that nearly 80 percent of the profiles had surface reflectivities equal to the profile maximum.

Since at short range the near-surface reflectivity value would have the greatest weight in the fan beam averaging, the prevalence of the near-surface reflectivity maximum feature in Konrad's storm core profiles suggests that minimal or no reflectivity adjustment is needed at short range much of the time. At longer ranges, the low beam reflectivity estimate is only representative of the near-surface reflectivity when the near-surface reflectivity feature is sufficiently deep to substantially fill the radar beam. Most of Donaldson's median profiles and Konrad's mean profiles show nearly constant reflectivity with altitude below approximately 5 km, with reflectivities decreasing above. ASR reflectivity estimates for such profiles would require little correction.

In order to investigate the relationship of storm vertical structure and fan beam radar reflectivity estimation, it is necessary to examine individual vertical reflectivity profiles taken through a variety of locations within the storms -- not just through the storm cores. When this was done, we found that the shapes of the individual reflectivity profiles often differed markedly from the median and mean storm core profiles. An illustration of why these differences occur between the mean profiles and individual profiles can be seen in Figure 6. Figure 6a shows a set of three artificial reflectivity profiles normalized by their own maximum reflectivity and whose shapes are comparable to profiles commonly observed at different stages during the evolution of a thunderstorm. The corresponding mean profile is

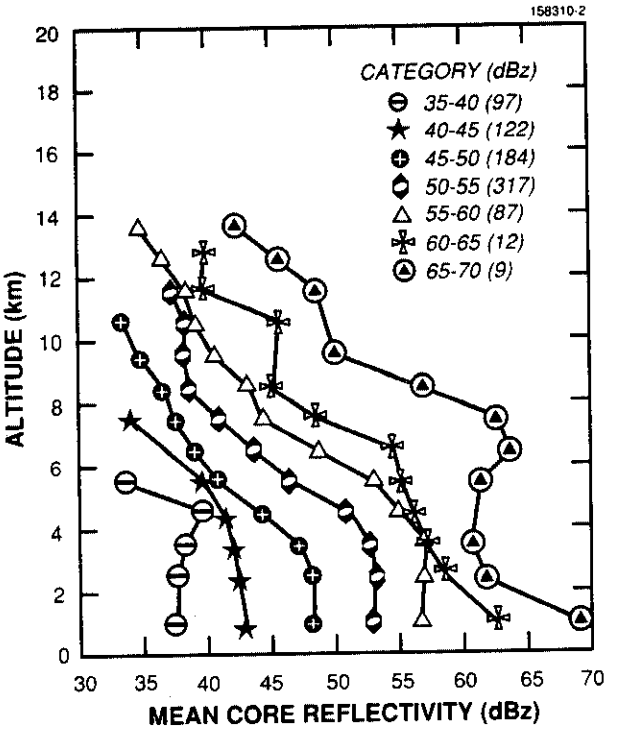

Figure 5. Profiles of mean core reflectivity for various categories of rainshowers. Number of cells in each category is shown in parentheses. (From Konrad, 1978.)

Figure 6b. The deep layer of near-maximum reflectivity apparent in the mean profile is an artifact arising from the averaging of profiles with peaks at varying altitudes. Figure 7 plots the differential reflectivity between the uncorrected ASR-9 fan beam equivalent reflectivity Z_{asr} and the vertical reflectivity profile maximum projection Z_{max} (a useful 2-D reflectivity representation for air traffic control purposes in summertime convective storms). Relative to the mean profile, a significantly greater differential reflectivity is seen between Z_{asr} and Z_{max} computed from the individual profiles in Figure 6, especially at those ranges where the nose of the radar beam intercepts the storm profile above or below the profile peak. The ASR-9 may underestimate the intensity associated with these small scale peaks to varying degrees depending on the relative location of these peaks with respect to the antenna gain pattern.

In a previous study (Weber, 1986), radar reflectivity data from summertime convective storms in New England and Oklahoma were used to derive the ASR-9 beam filling loss adjustments as a function of range for each weather level (Figure 8). The adjustments were derived by computing the reflectivity scaling factor which minimized the error between the uncorrected ASR-9 weather reflectivity and the desired (maximum) reflectivity. He found that the magnitude of the required threshold adjustments increased with range for all levels, consistent with expectations based on the shapes of Konrad's (1978) mean profiles. The magnitude of the adjustments tended to be larger for weather levels 3-6 than for weather levels 1-2 due to larger variations in relative reflectivity in the vertical profiles of the more severe storms. The work in this report follows the computational method outlined by Weber, but expands significantly the scope of the data set.

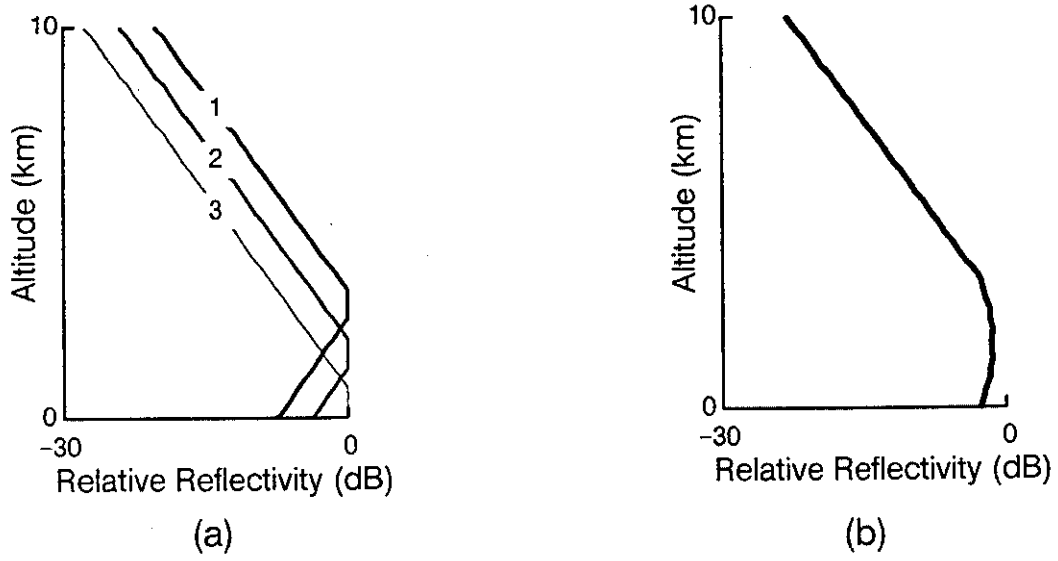

Figure 6. Illustration of vertical reflectivity profile averaging process: (a) Superimposed set of normalized profiles, (b) Mean profile derived from averaging of normalized profiles.

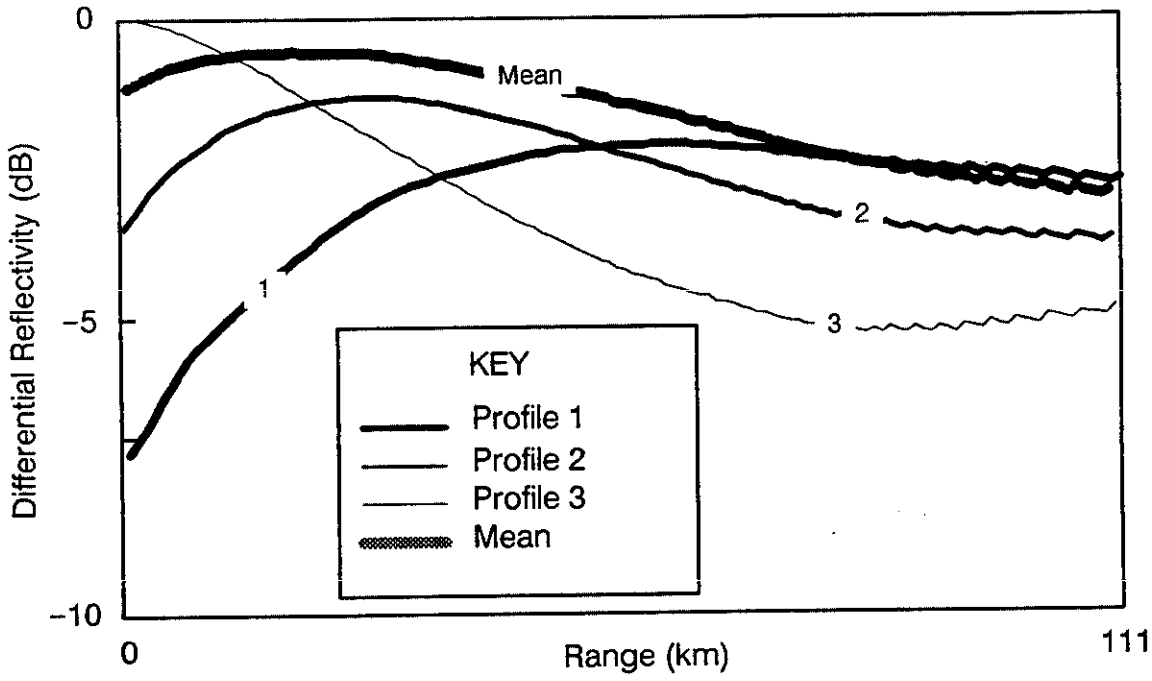

Figure 7. Reflectivity difference between the uncorrected ASR-9 reflectivity (low beam) and the vertical profile maximum for the three profiles and their mean shown in Figure 6.

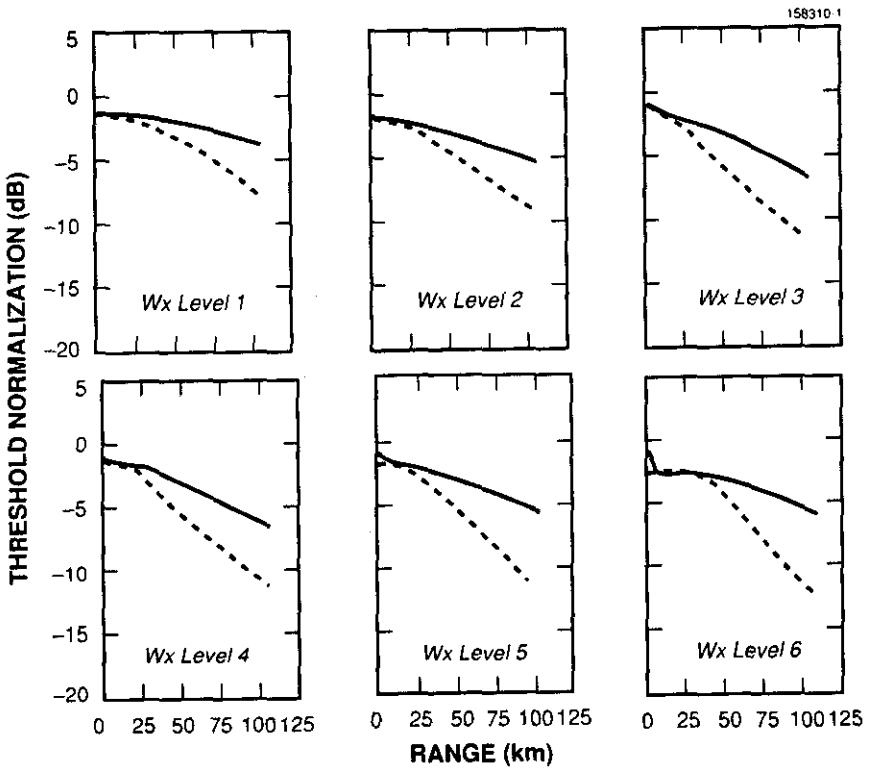

Figure 8. ASR-9 6-level weather threshold normalizations for New England convective storms. Solid and dashed curves are low and high beam adjustments, respectively. (From Weber, 1986.)

1.2. ASR-9 WEATHER CHANNEL BEAM FILLING LOSS ADJUSTMENTS - CURRENT IMPLEMENTATION

A block diagram of the ASR-9 weather channel processor is presented in Figure 9. A more complete description can be found in *The ASR-9 Weather Channel Test Report* (Puzzo et al., 1989). Input time series (I,Q) data are first passed through a bank of four FIR clutter filters. One of the filters is all-pass, while the other three provide increasing ground clutter rejection. A clear day map of the ground clutter distribution is used to adaptively select the narrowest high-pass filter that will adequately suppress ground clutter at each range-azimuth cell for each of the six NWS levels. The magnitudes of the filter outputs are then passed to the six-level thresholding function. The weather thresholds are adjusted, taking account of receive beam (high or low), range, STC, and signal polarization. The range-dependence allows the reflectivity thresholds to include compensation for reflectivity estimate bias arising from non-uniform filling by precipitation of the broad fan beam. Weather threshold crossings are then sent to a three-stage smoothing and contouring function which performs temporal and spatial filtering to reduce reflectivity estimate variance and produce a more stable display from scan to scan.

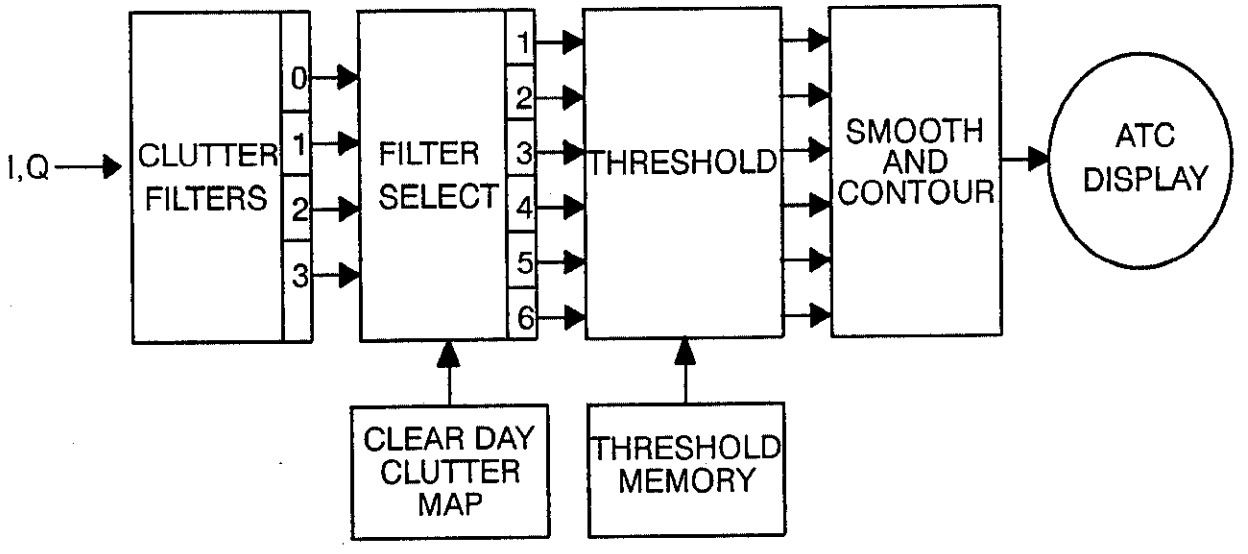

Figure 9. ASR-9 six-level weather channel block diagram.

An initial beam filling loss threshold adjustment has been currently implemented on the ASR-9 using a "representative" model profile of relative reflectivity. The model assumes a layer of constant maximum reflectivity extending from the surface to 4 km, with a 3 dBZ per km decrease above 4 km. The model profile and the resulting adjustment curves are shown in Figure 10. The shape of the model profile is similar to the mean profile shapes derived by Konrad (1978) and the majority of profiles computed by Donaldson (1961), shown in Figure 5. Figure 10 shows no correction at near range, which means that the ASR-9 reflectivity report will remain biased at short range for any instance of an elevated

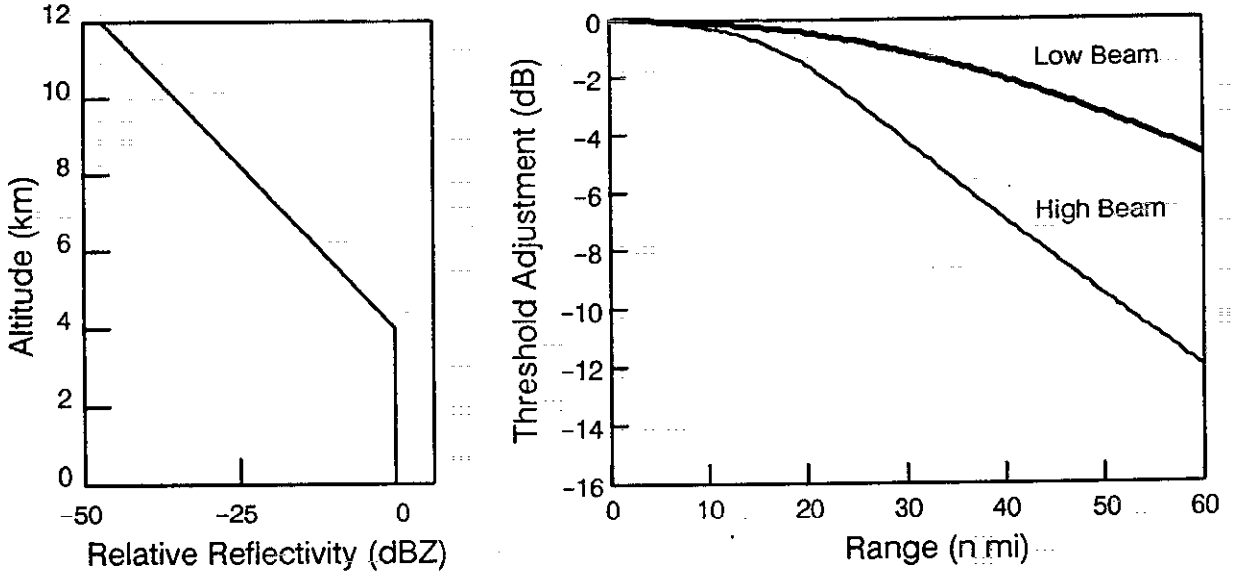

Figure 10. Current ASR-9 reflectivity profile model (left) and corresponding threshold adjustments (right).

layer of high reflectivity, such as the hail storm profiles shown in Figure 4. A theoretical problem with the current model is that while mean profiles are characterized by deep regions of maximum reflectivity, most observed reflectivity profiles are characterized by shallow maximum reflectivity features whose altitude placement and extent change with time. Thus, the reflectivity threshold adjustments suggested by the current model may result in an underestimate of the maximum storm intensity at any altitude.

2. DATA ANALYSIS METHOD

2.1. DATA SET

In order to study potential regional differences in reflectivity profile shapes, it was necessary to choose a variety of geographic locations for the analyses. Past thunderstorm research has suggested distinct regions of activity (Easterling and Robinson, 1985). For our work, five regions were identified and are shown in Figure 11. They are: East (E), Florida and South Plains (S), Midwest (M), High Plains (HP), and West (W). One site from each of the five regions was chosen for analysis, and they are indicated by filled circles in Figure 11. The sites are: Boston, Massachusetts; Huntsville, Alabama; Kansas City, Missouri; Denver, Colorado; and Seattle (Pt. Brown), Washington. For each of these sites, data were chosen to represent four types of precipitation systems whenever possible: stratiform (shallow widespread low reflectivity storm systems); frontal (bands of clouds originating at the juncture of cold and warm air masses); airmass (isolated convective activity); and severe (characterized by extensive vertical development and high reflectivities).

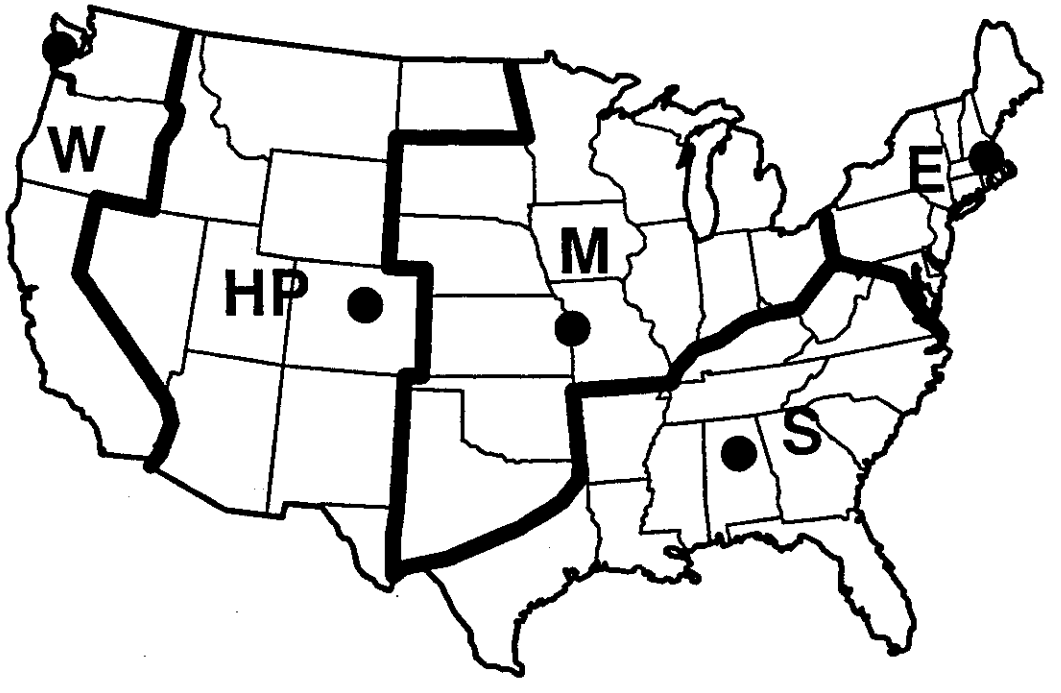

Figure 11. ASR-9 beam filling loss correction storm model regions.

The input data consisted of 273 volume scans distributed among the five sites. This resulted in over one million profiles to be used for calculating the beam filling loss corrections. The list of volume scans used from each site are given in Appendix A. Included are the date and start time of each scan, which may have taken anywhere from 2 1/2 to 10 minutes to complete. The number of PPIs comprising the volume scan (tilts) and the maximum tilt elevation angle are also noted. Volume scans were required to have a minimum scan angle below 2.0 degrees and to have a maximum scan angle sufficient to clear the tops of

the storms. In several cases, only data inside certain azimuth and range limits were used. This was done to avoid interference from residual ground clutter.

Table 1 lists characteristics of the radars which produced data used for this study. These data were collected in conjunction with a variety of field experiments. The CP-3 and CP-4 radars were operated by the National Center for Atmospheric Research (NCAR) during the CYCLES (Cyclonic Extratropical Storms) Project on the Washington Coast during January and February, 1982 (Hertzman and Hobbs, 1988). The MIT S-band radar, located at the MIT campus in Cambridge, Massachusets was used for an FAA-sponsored Lincoln Laboratory study of New England thunderstorms during the summer of 1983, as well as for on-going weather studies. The MIT C-band transportable radar system was operated under contract with the MIT Weather Radar Laboratory in support of FAA/Lincoln Laboratory field testing of the ASR-9 weather channel at Huntsville, Alabama during the summer of 1988. The FAA/Lincoln Laboratory (FL-2) S-band radar serves as a Terminal Doppler Weather Radar (TDWR) testbed radar and was used for TDWR operational testing and evaluation at Denver, Colorado in 1988 and at Kansas City, Missouri in 1989.

Table 1.
Radar Characteristics

	NCAR CP-3 Radar	NCAR CP-4 Radar	MIT S-band Radar	MIT C-band Radar	FL-2 Radar
Gate spacing (m)	150	150	250	250	120
Pulse width (μs)	1.0	1.0	1.0	1.0	0.65
Wavelength (cm)	5.45	5.49	10.5	5.4	10.5
Polarization	Horizontal	Horizontal	Horizontal	Vertical	Horizontal
PRF (Hz)	1000	1000	541	924	700-1200
Beamwidth (deg)	1.1	1.1	1.45	1.4	0.96
Rotation rate (s/360 deg)	12	12	35	25	30

2.2. CONSTRUCTION OF VERTICAL REFLECTIVITY PROFILES

The first step in deriving the necessary weather channel threshold adjustments consisted of constructing smooth vertical profiles of reflectivity from the pencil-beam radar volume scan data. Each volume scan consisted of a series of full-circle or sector PPI scans containing between five and 20 constant elevation tilts. Selected azimuth sectors of these volume scan data were mapped onto a cylindrical coordinate grid having a range radius of 60 nmi (111 km) and a height of 65620 ft (20 km). Azimuthal and range granularity of the cylindrical grid were set to 1.41° and 0.5 nmi (0.926 km) respectively, while vertical granularity was 1641 ft (0.5 km). A profile cylinder generated from a single full-circle volume scan could therefore contain as many as 30,720 individual vertical reflectivity profiles. Figure 12

This report most closely resembles reports produced by the horizon-scanning NWS pencil beam radar. Although this parameter would be fairly representative of current conditions immediately above the airport, it would fail to indicate potentially significant reflectivity development aloft. Such elevated reflectivity features often precede the onset or intensification of precipitation on the ground by several minutes and could provide useful advance warning.

A more conservative representation is the vertical maximum reflectivity product:

$$Z_{max}(R,\theta) = MAX[\, Z(R,\theta,H);\, 0 \leq H < \infty \,] \quad . \tag{3}$$

It is sensitive to regions of strong intensity regardless of their altitude and vertical extent. Hence, it is a an indication of the most intense precipitation that could be encountered by an aircraft at any altitude. It is, however, insensitive to the percentage of the storm's vertical structure that has reflectivity near the maximum intensity level. Hence, a shallow region of high reflectivity would be represented by the same Z_{max} value as a deep region of comparable reflectivity. This should not present serious operational consequences, since the indication of hazardous storm conditions at any altitude, regardless of the vertical extent of the hazard, could be construed as sufficient cause for avoidance.

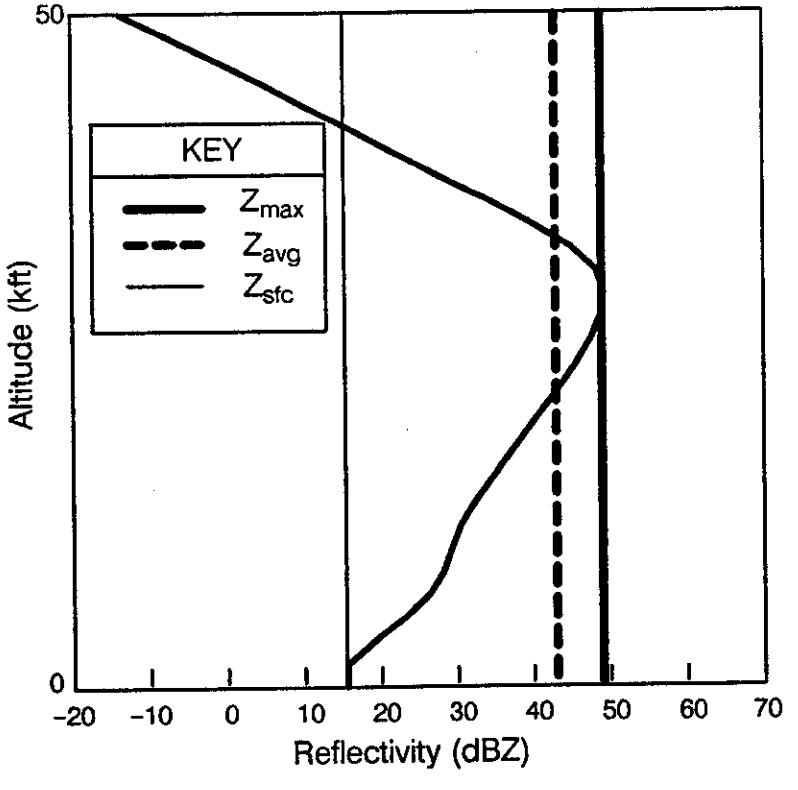

Figure 14. Vertical reflectivity profile through Denver thunderstorm on July 3, 1987 at azimuth 162.0°, range 26.5 nmi. Vertical lines indicate Z_{max}, Z_{avg}, and Z_{sfc} for the profile shown (see key).

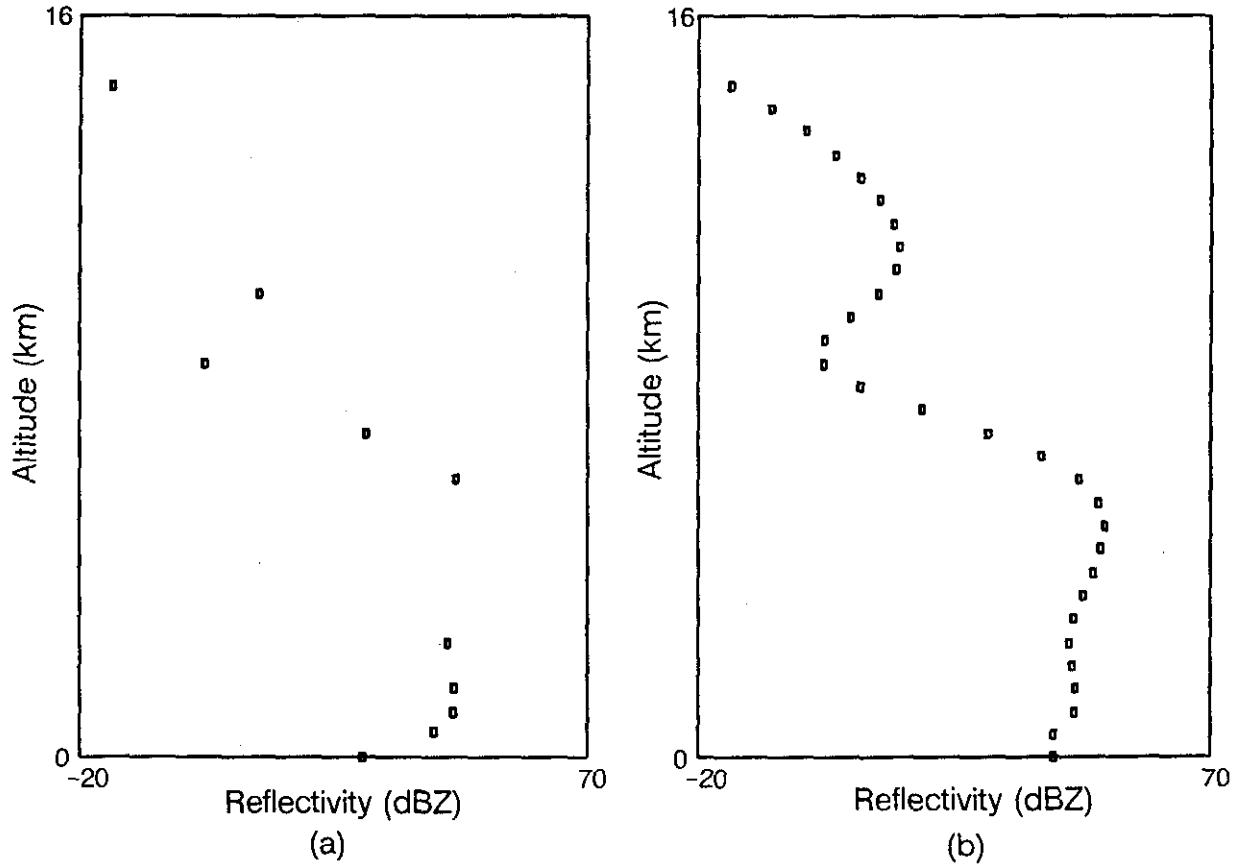

Figure 13. Vertical reflectivity profile (a)before and (b)after filtering and filling.

be used to characterize the storm profile, depending on the parameterization chosen. The elevated reflectivity peak seen in the figure is a relatively common characteristic of the profiles we examined. These peaks typically form aloft during initial storm development and then descend as the storm matures and dissipates. This profile serves as a useful example for illustrating the representativeness of various parameterizations of the profile. For example, the desired reflectivity report could be defined as the average reflectivity over the depth of the storm:

$$Z_{avg}(R,\theta) = \int_{H_1}^{H_2} Z(R,\theta,H)\, dH \,. \qquad (1)$$

H_1 = echo base altitude
H_2 = echo top altitude

This storm-average reflectivity most closely resembles the parameter reported by the ASR-9 weather channel, especially if the beam is filled with precipitation.

Alternatively, we may define a near-surface reflectivity product:

$$Z_{sfc}(R,\theta) = Z(R,\theta,H=0) \,. \qquad (2)$$

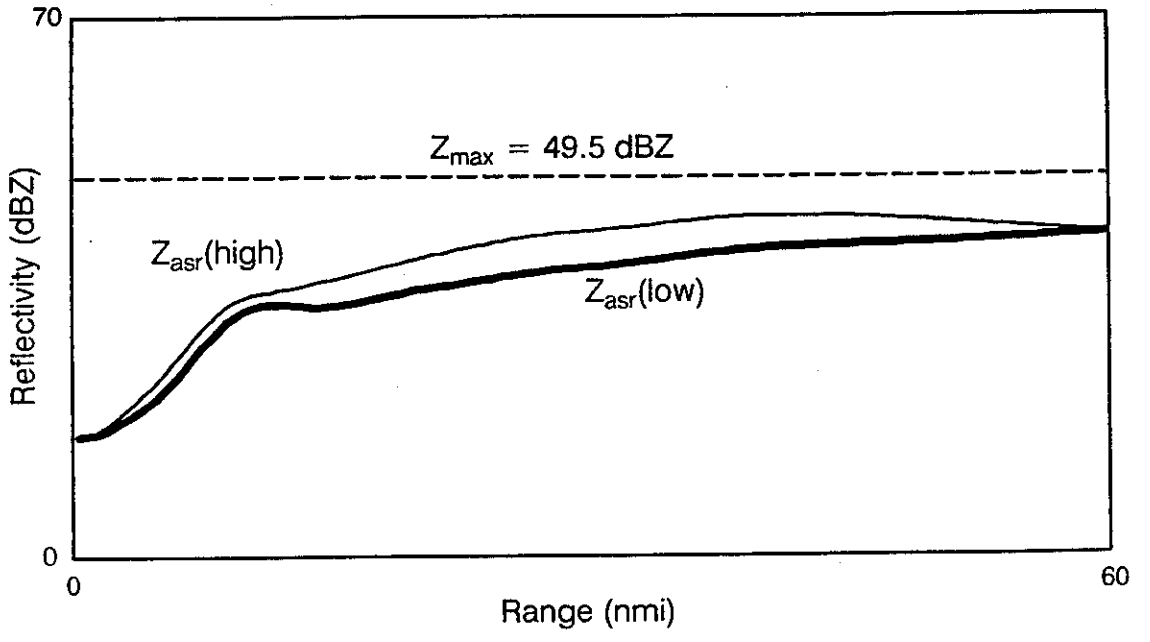

Figure 15. Z_{max} and Z_{asr} (low and high beams) computed from reflectivity profile of Figure 14. An ASR antenna tilt of 2.0° was assumed for computation of Z_{asr}.

2.5. CALCULATION OF WEATHER CHANNEL THRESHOLD ADJUSTMENTS

Recall that the weather thresholds are stored in the weather channel processor memory as functions of range, receive beam, and weather level. The Z_{asr}(R,beam,wx level) curves and the Z_{max} values provide the information needed to derive the required threshold adjustments. Weber [1986] proposed a method for calculating the threshold adjustments by computing the reflectivity scaling factor η which minimizes the mean square error ϵ between Z_{max} and Z_{asr} over the ensemble of profiles $\{p_1, p_2, \ldots, p_{N-1}, p_N\}$:

$$\epsilon^2(\text{R,beam,wx level}) = \sum_{p=1}^{N} \left[\frac{Z_{max} - \eta Z_{asr}(\text{R,beam})}{Z_{max}} \right]^2 . \qquad (6)$$

The scaling factor which minimizes the error is given by:

$$\eta(\text{R,beam,wx level}) = \sum_{p=1}^{N} (Z_{asr} / Z_{max}) \Big/ \sum_{p=1}^{N} (Z_{asr}^2 / Z_{max}^2) . \qquad (7)$$

Equation (7) was used to calculate η (the reciprocal of the required threshold adjustment) as a function of range for both receive beams and for each of the six NWS weather levels. The weather level of a profile was defined to be the NWS level corresponding to Z_{max}.

While Z_{max} provides a useful measure of intensity in summertime convective storms, it may not be appropriate for characterizing the intensity of wintertime stratiform precipitation, since it is overly sensitive to bright-band effects (an enhanced reflectivity layer associated with the region of ice-to-water phase change) often observed in these types of storms.

Some of the vertical reflectivity profiles we examined were characterized by a sharp elevated peak. For these profiles, the vertical maximum reflectivity as defined by equation (3) was significantly larger than values at other altitudes, including those in relatively close proximity. The absolute profile maximum reflectivity would therefore be unrepresentative of conditions likely to be encountered by an aircraft. For these reasons, we chose to construct a less sensitive maximum reflectivity parameter which was formulated as the average of the three (M = 3) highest reflectivity values in the sorted (by reflectivity) distribution of N profile values $\{Z_1, Z_2, ..., Z_{N-1}, Z_N\}$:

$$Z_{max}(R,\theta) = \frac{1}{M} \sum_{i=0}^{M-1} Z(R,\theta)_{N-i} \qquad (4)$$

For the majority of profiles, which are characterized by smooth reflectivity gradients, this formulation produces estimates of Z_{max} which are similar to those produced using equation (3).

2.4. COMPUTATION OF Z_{ASR} FROM VERTICAL REFLECTIVITY PROFILES

For each of the reflectivity profiles in the cylinder, the equivalent ASR-9 reflectivity (Z_{asr}) was computed at 4 nmi range intervals from 0 to 60 nmi, using:

$$Z_{asr}(R,\text{beam}) = \frac{\int Z(R,\phi)\, B_t(\phi)\, B_r(\phi)\, d\phi}{\int B_t(\phi)\, B_r(\phi)\, d\phi} \qquad (5)$$

The implementation of equation (5) was as follows: Each vertical reflectivity profile was first integrated over elevation angle, weighting each of the individual profile values $Z(R,\phi)$, by the relative ASR-9 two-way beam power $B_t(\phi)B_r(\phi)$ for that elevation angle. This total integrated reflectivity, represented by the numerator of equation (5), was then normalized by the total relative antenna power (the denominator of equation (5)) to yield Z_{asr} at that particular range gate. The entire Z_{asr} calculation was then repeated (using the same profile) at 4 nmi increments for each of the two receive beams. Figure 15 is a plot of Z_{asr} and Z_{max}, computed using the single reflectivity profile of Figure 14. The range-dependent differences between Z_{asr} and Z_{max} define error curves (one curve for each receive beam) which represent the amount of weather threshold adjustment required to bring Z_{asr} into agreement with Z_{max}.

3. RESULTS

3.1. Site/Level Specific Threshold Adjustment Curves

Threshold adjustments as a function of range were computed separately for each NWS level at each of the five locations identified in Section 2.1. For each site a data set was chosen to include a variety of storm types, including airmass thunderstorms, frontal convection, stratiform rain, and severe thunderstorms. The computations followed the method described in the last section. Regardless of the observational range of the profile, each profile was used to compute the ensemble corrections at all ranges for both beams of the ASR-9 radar. The result is a set of curves indicating the threshold adjustment required as a function of range, with one curve for each beam, weather level, and site, for a total of 60 curves. Threshold adjustment curves were generated for each weather level in which there was a minimum of 100 input profiles. These curves are shown in Figure 16 – Figure 20. An insufficient number of profiles precluded accurate determination of threshold adjustments for weather levels 4–6 for Seattle, and weather level 6 for Huntsville. Although the ASR-9's level 1 reports are not compensated for beam filling losses, the level 1 adjustments are included for completeness. In general, the amount of adjustment varies from near 0 dB at the radar to approximately 6 dB for the low beam and 11 dB for the high beam at 60 nmi range for each of the weather levels.

The most striking feature of these graphs is the similarity of the curves between the different weather levels and sites. The only site whose adjustments differed slightly in magnitude from the other four was Seattle, with Seattle weather requiring a greater correction most notably in the high beam. This may be partly due to reduced filling of the ASR-9 beam by the vertically limited cloud structures associated with the stratiform storm systems typical of the data from Seattle, but it may also be related to the presence of anomalously high reflectivity regions associated with ice/liquid phase transitions at the freezing level (bright-band). The bright band in the data tended to be located near 9,800 ft (3 km) altitude, which is below the lower 3 dB edge of the high beam beyond 30 nmi. This resulted in anomalously large corrections at long range for the high beam. The operational impact of these larger corrections must be considered.

3.2. Single U.S. Threshold Adjustment Curve

The similarity between weather levels and regions of the United States suggests that a single correction for each of the two beams might be applicable to all sites and weather levels, with the possible exception of storms producing bright band radar echoes. To investigate this, a single U.S. correction was created by using Equation 7 to derive the optimal threshold adjustment for an ensemble consisting of profiles from all weather intensity categories and from all five regions. A linear least squares fit was then made to the resulting low and high beam threshold adjustment data. The equations for the best fit lines for the two beams were found to be:

$$\text{U.S. Low Beam Adjustment (dB)} = -0.1193 \times \text{range (nmi)} - 0.2371 \quad (8)$$

$$\text{U.S. High Beam Adjustment (dB)} = -0.2005 \times \text{range (nmi)} - 0.4836 \quad (9)$$

with correlation coefficients of 0.999 and 0.995 for the low and high beams, respectively.

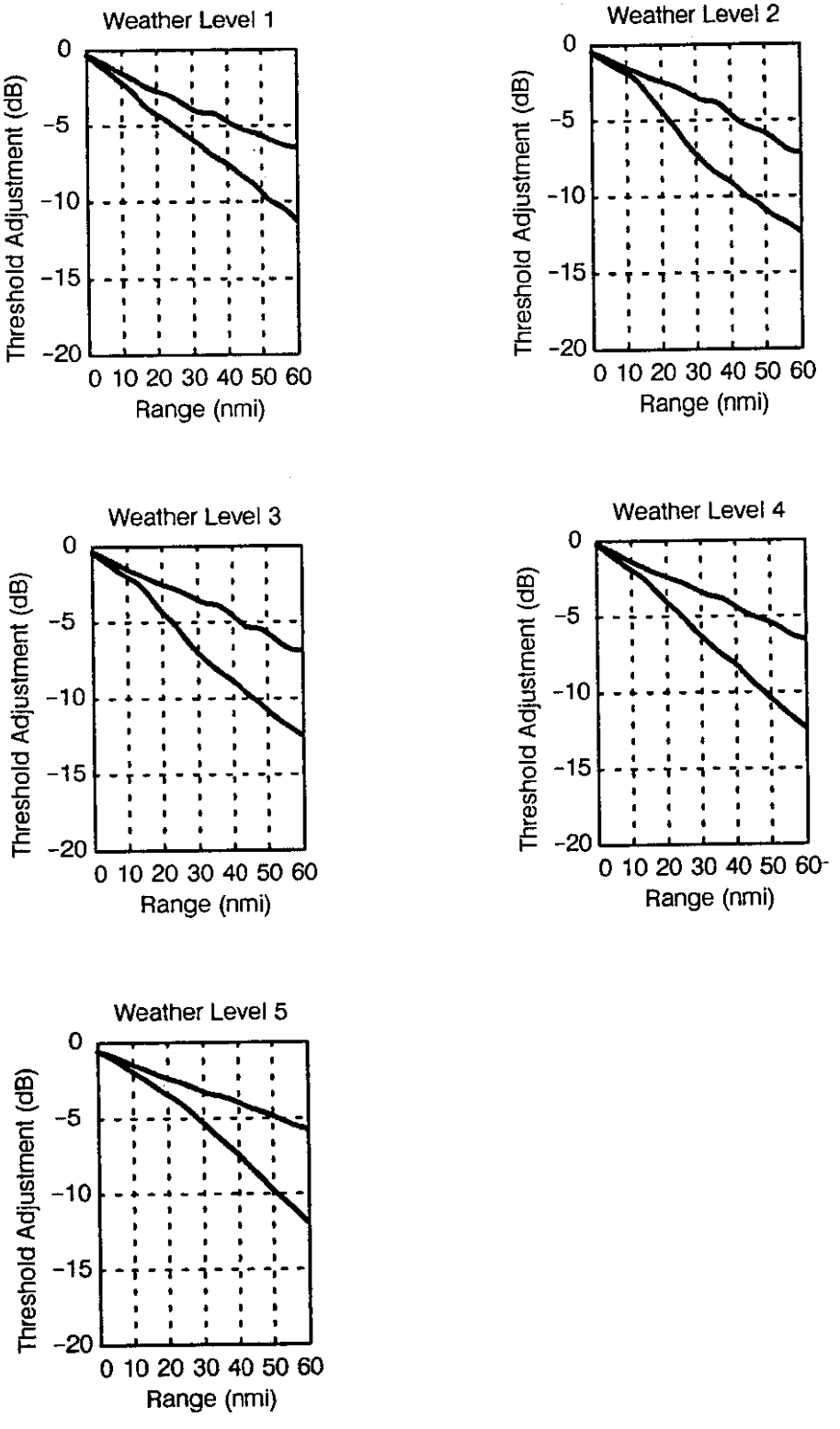

Figure 17. Threshold adjustments as in Figure 16, but for the Huntsville data set.

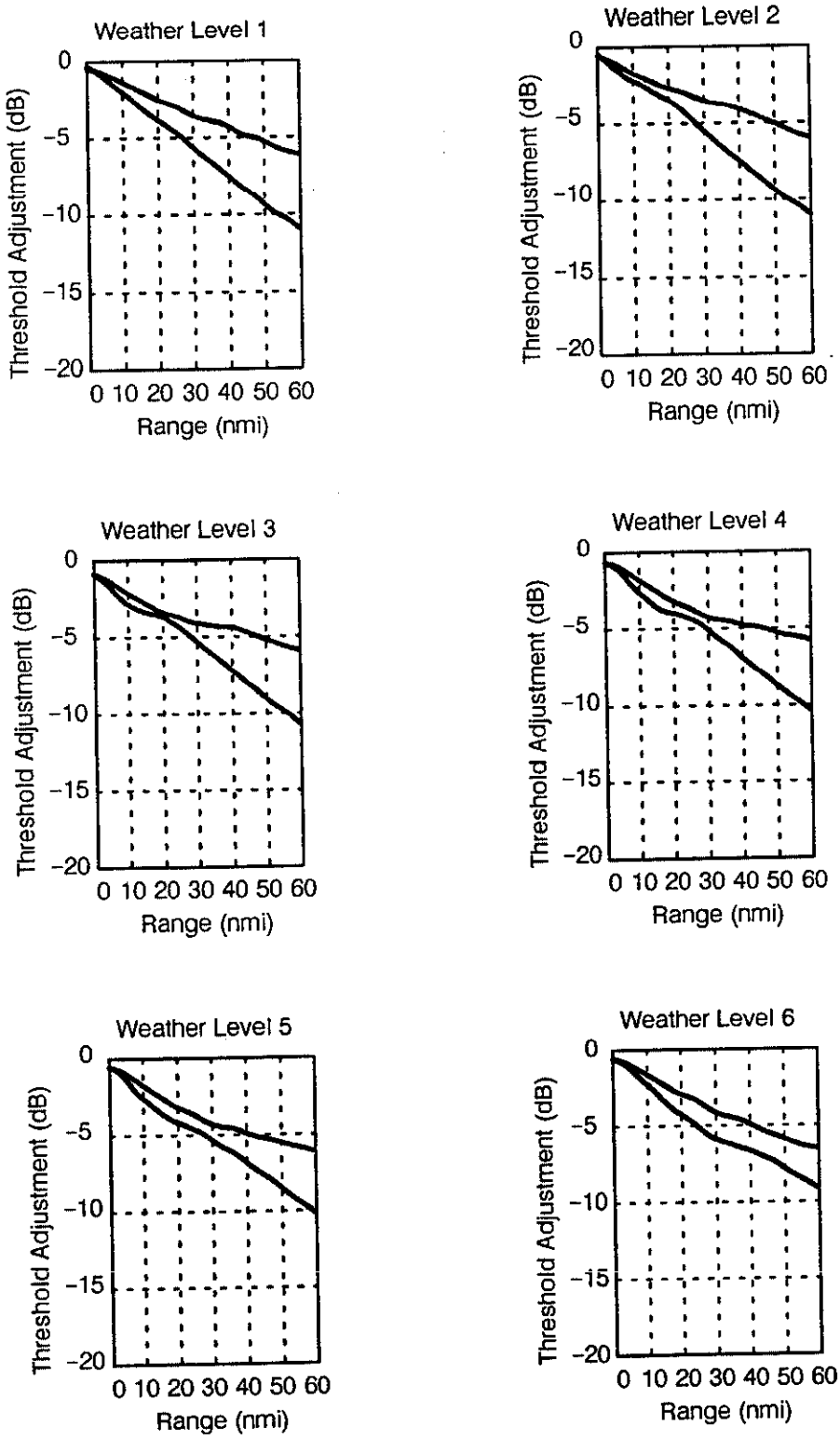

Figure 16. Threshold adjustments necessary to minimize the report error of the ensemble of profiles comprising each weather level in the Boston data set. Upper curve is for the low beam, lower curve for the high beam.

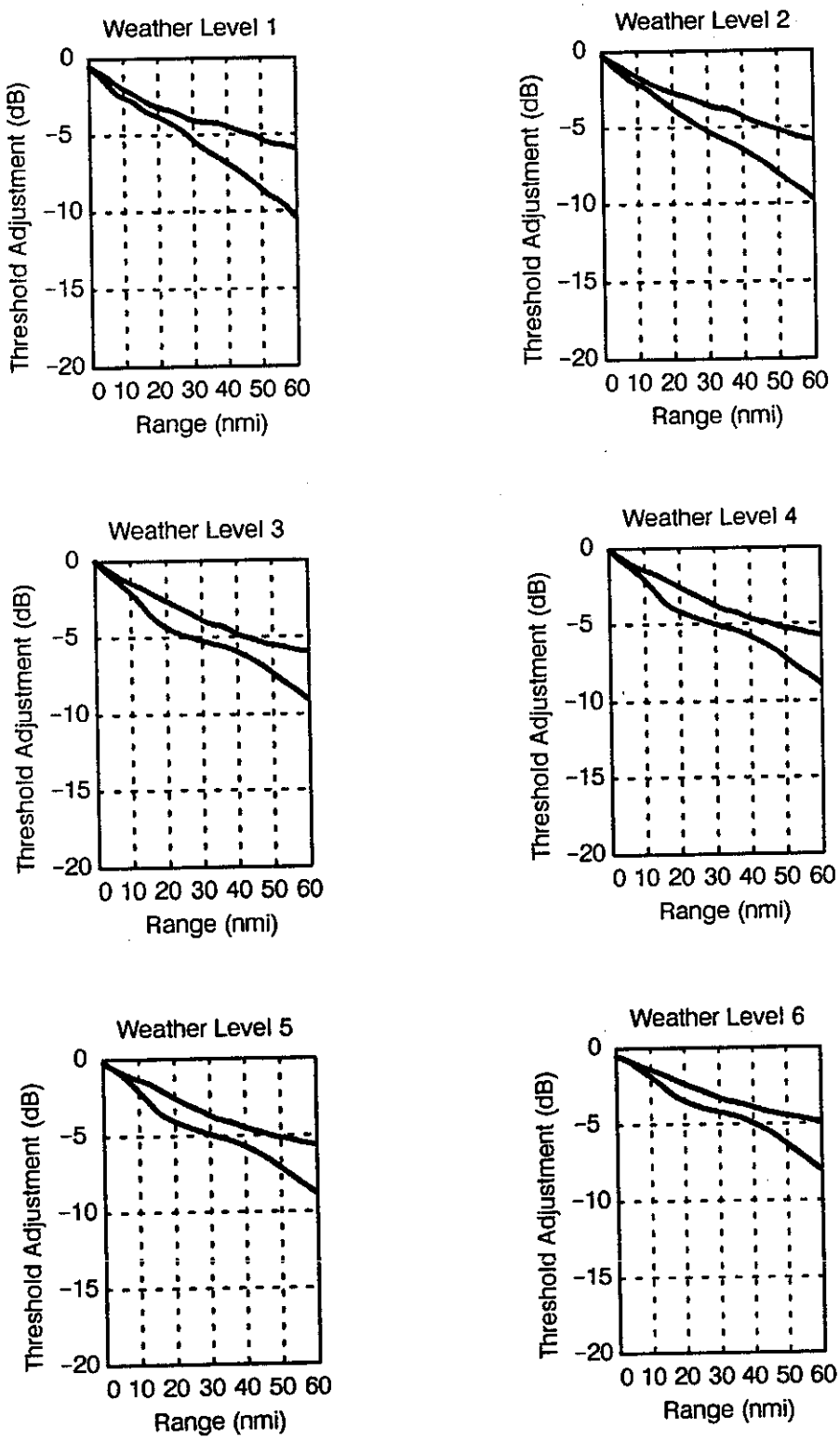

Figure 19. Threshold adjustments as in Figure 16, but for the Denver data set.

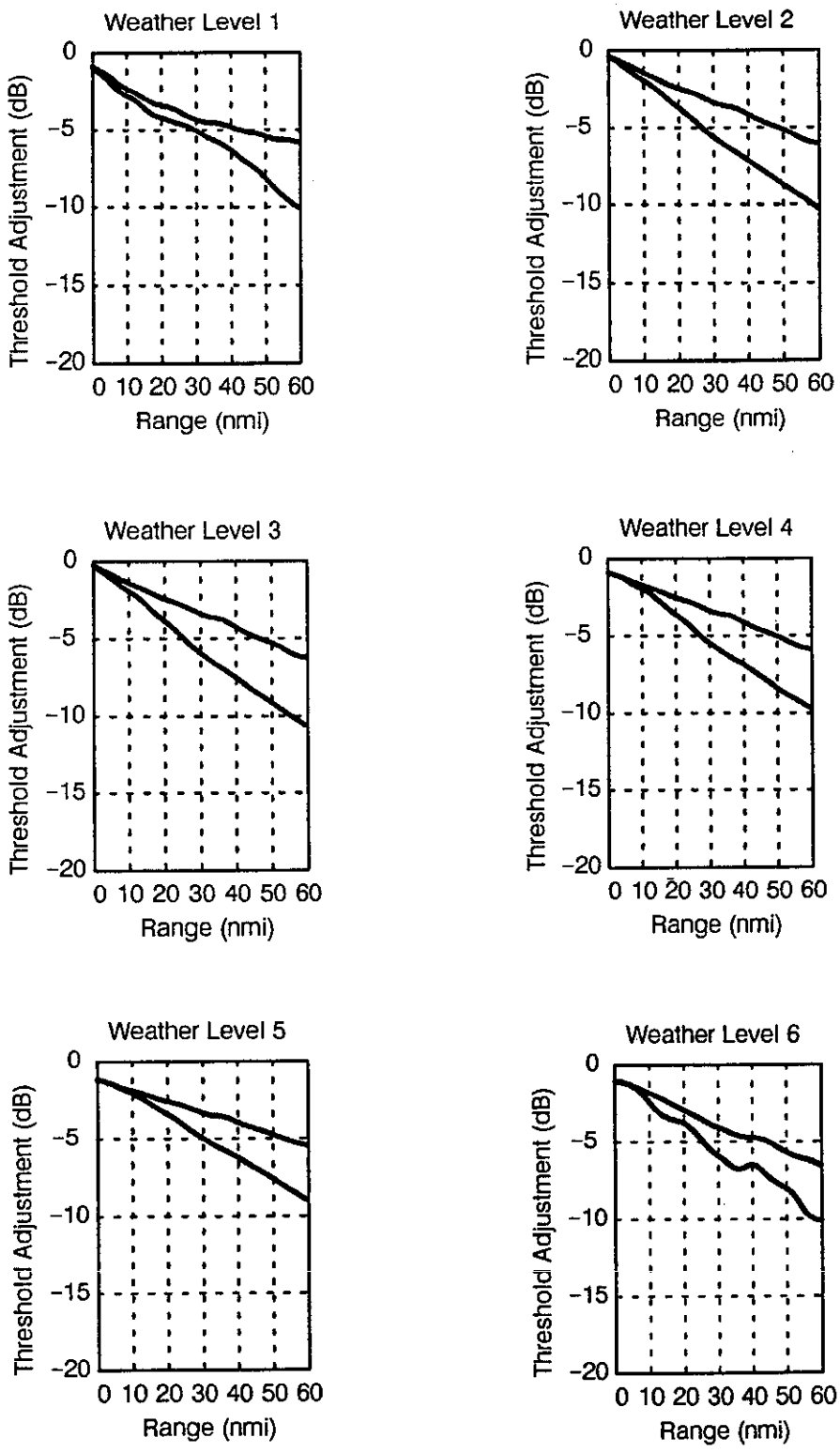

Figure 18. Threshold adjustments as in Figure 16, but for the Kansas City data set.

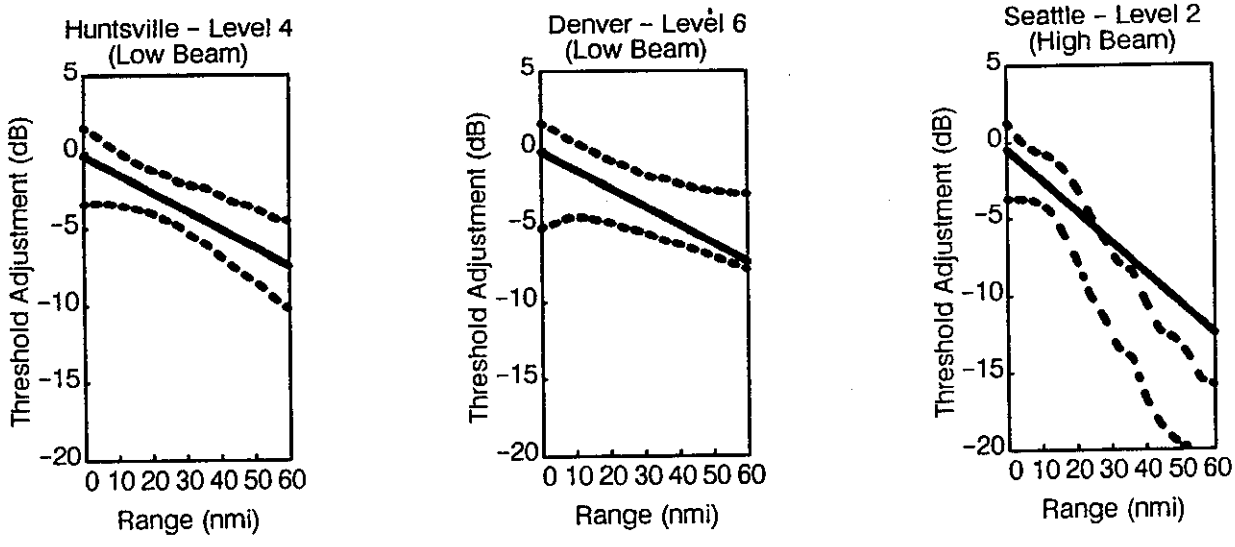

Figure 21. Relative placement of U.S. threshold adjustment curve (solid) with respect to upper and lower rms error bounds of site/level specific adjustment curves (dashed).

cause the ASR–9 level 1 threshold is tied to the system noise level and is not adjusted for beam filling losses, performance statistics were generated only for those profiles in weather level categories 2–6.

The metric chosen to quantify how well the threshold adjustments performed was the percentage of profiles whose reported weather level matched the weather level corresponding to Z_{max}. Figure 22 shows a comparison of the success of the threshold adjustments at reporting the maximum reflectivity at any altitude. The profiles were grouped in 10 nmi bins in order to evaluate the effect of range on the success of the corrections. Although adjustments were computed and implemented for both beams, only the more operationally significant low beam results are presented here. A similar amount of improvement was noted in the high beam reports. Uncorrected ASR–9 report accuracy is shown with a solid line and filled squares. Accuracy decreased from about 70 percent at close range to only 20 percent at far range. Results using the current ASR–9 beam filling loss correction (Figure 10) are shown with a dashed line and filled circles. At close–range, adjustments prescribed by the current model are minimal, so little improvement is seen between the uncorrected reports and those corrected with the current model. At far range, the current adjustments provide approximately 25 percent improvement in report accuracy.

Results of corrections using the U.S. threshold adjustments are shown with a dotted line and x's. Correction of ASR–9 reports using these threshold adjustments resulted in a substantial improvement in report accuracy relative to uncorrected reflectivities, ranging from approximately 10 percent at close range to over 60 percent at maximum range. The success of the U.S. adjustment curve is further illustrated in Table 2 which shows the distribution of weather report errors versus profile range for the entire test data set. Numbers in the upper left of each box represent the percentage of uncorrected profiles in the noted range bin whose reports differ from Z_{max} by −1, 0, +1, +2, and +3 NWS levels. For example, the −1 report error category represents over–correction by one NWS level. Numbers in the

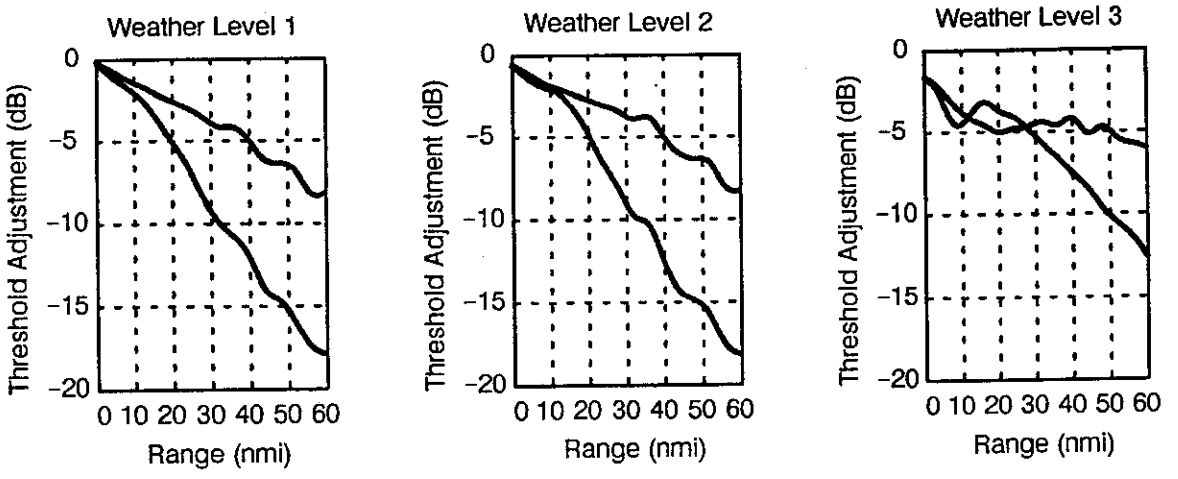

Figure 20. Threshold adjustments as in Figure 16, but for the Seattle data set.

The resulting U.S. threshold adjustment curve for each beam generally falls between the corresponding upper and lower rms error bounds for the various site/level specific threshold adjustments. The leftmost and center graphs of Figure 21 typify the relative placements of the U.S. curve with respect to the site/level specific error bounds. The U.S. adjustment is indicated with solid lines, while dashed lines indicated the rms error bounds. The only exceptions to this typical relationship were found in the threshold adjustments derived from the Seattle data, an example of which is shown on the right of Figure 21. Here, the U.S. adjustment curve lies above the level 2 upper error bound at ranges greater than 25 nmi. The exceptions from Seattle do not invalidate the U.S. adjustment curve for two reasons. First, as noted previously, the prevalence of bright-band in the Seattle data produced excessively large threshold adjustments. The U.S. adjustment curve represents a more appropriate treatment for convective storms. Second, the only notable region of discrepancy is that shown in the example of Figure 21. This discrepancy occurred with the high beam at long range, where the low beam is used under normal operations. Because the U.S. adjustment curve falls within the error bounds for 49 of the 52 site/level specific adjustment curves and because the exceptions do not invalidate the U.S. threshold adjustment curve, we believe that the U.S. threshold adjustment curve is appropriate for operational implementation.

3.3. Correction Performance

Using our ASR-9 simulation facility, performance of the U.S. (Eq. 8 and 9) threshold adjustments was evaluated. The test data set was comprised of the same pencil-beam radar volume scan data used to compute the corrections. Corrections were applied to the individual profiles only at their original observational ranges during this statistical evaluation of correction performance.

Corrected ASR-9 weather reports were generated by first obtaining the equivalent fan beam reflectivity Z_{asr} for each profile using the method outlined in Section 2.4. The appropriate threshold adjustment for the observational range of the profile was used to lower the six NWS reflectivity thresholds. The Z_{asr} estimate was then thresholded against the adjusted thresholds to obtain the corresponding corrected six-level weather report Z_{six}. Be-

Table 2.
Distribution of Relative Weather Report Errors Versus Profile Range for the Entire Test Data Set.*

Beginning Range of Radar Data Volume (nmi)	Relative Report Error (NWS Levels)				
	−1	0	+1	+2	+3
0	0.4 0.9	69.2 77.5	27.6 19.3	2.5 2.1	0.3 0.3
10	0.0 0.7	49.4 73.0	45.9 22.8	4.2 3.3	0.5 0.2
20	0.0 1.5	45.6 83.7	53.0 14.3	1.3 0.5	0.1 0.0
30	0.0 2.5	40.3 86.2	58.3 11.1	1.4 0.1	0.0 0.0
40	0.0 3.1	29.7 83.4	69.2 13.5	1.1 0.0	0.0 0.0
50	0.0 3.3	20.3 82.4	77.3 14.1	2.4 0.1	0.0 0.0
Overall (0 – 60 nmi)	0.1 1.6	47.9 79.9	49.4 17.0	2.4 1.5	0.2 0.1

* Numbers in the upper left of each box represent the percentage of uncorrected profiles in the noted range bin whose reports differ from Z_{max} by −1, 0, +2, and +3 NWS levels.

3.4. Causes of Threshold Adjustment Failure

The results presented in Table 2 indicate that 98 percent of the profiles in the test data base were assigned a corrected weather level within one level of the desired reflectivity report (where the low beam was used at all ranges). Examination of the remaining 2 percent of the profiles indicates that nearly 70 percent of these profiles were located in the vicinity of severe storms (maximum reflectivity > 50 dBZ, echo tops > 35,000 ft) (Table 3). In order to understand the connection between severe storm structure and weather channel threshold adjustment failure, we examined data taken during a severe storm event which occurred on September 5, 1987 at Denver.

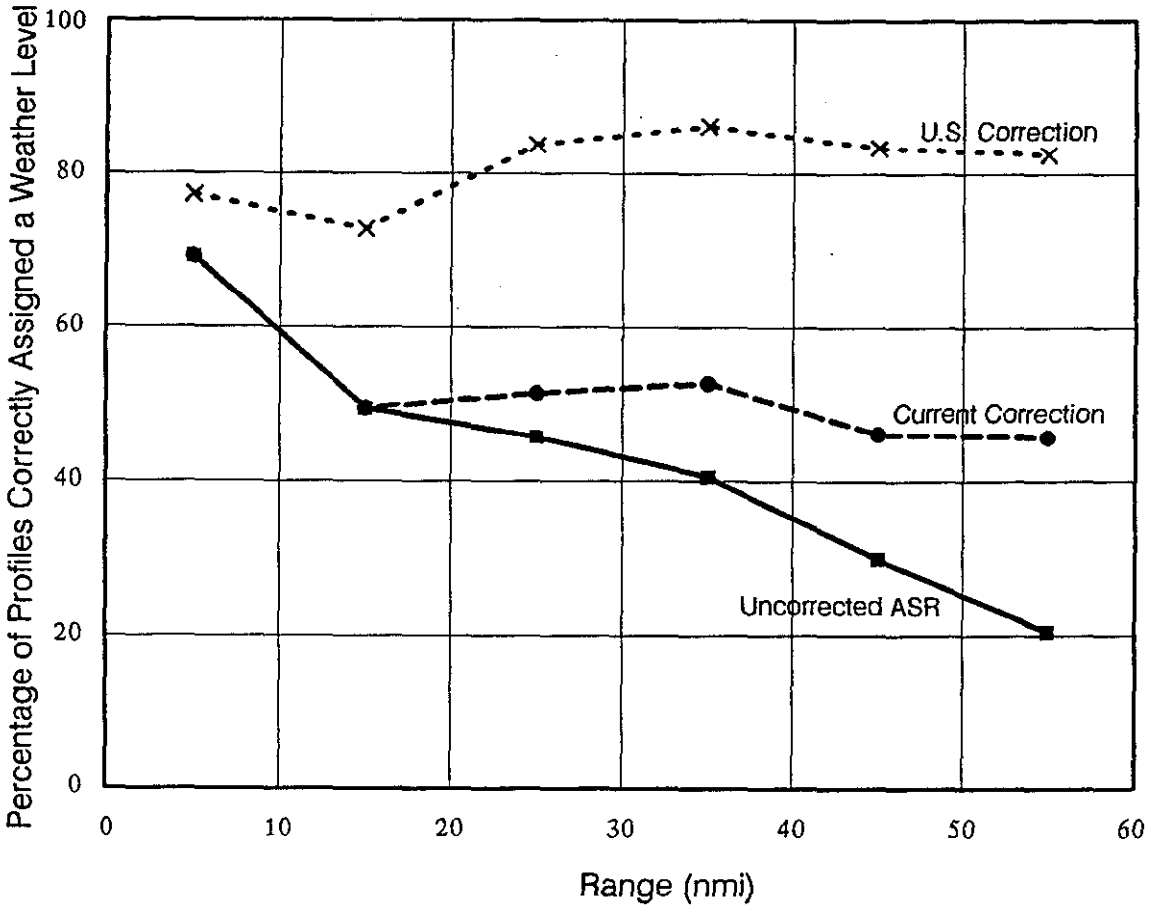

Figure 22. Percentage of cells in weather levels 2 through 6 for all sites that are correctly quantized. Solid line with filled boxes represents uncorrected quantization of ASR reported reflectivity. Dashed line with circles represents quantizations adjusted with current correction. Dotted line with x's represents quantizations adjusted with a single U.S. correction for all sites and weather levels.

lower right of each box represent similar statistics for profiles corrected using the U.S. threshold adjustment curve. After adjustment, nearly 80 percent of the profiles were correctly assigned a weather level, with an additional 17 percent underestimated by one weather level. Overestimates were quite uncommon — less than 2 percent of the corrected profiles exceeded the desired report level. Less than 2 percent of all profiles were underestimated by more than one level, most of these occurring at close ranges. A discussion of causes for the significant underestimation of some of the profile intensities will be presented later.

Figure 23 summarizes average weather report error for uncorrected and corrected ASR–9 reports. Since the majority of corrected profiles were within one level of Z_{max}, the average error is approximately representative of the fraction of profiles where the corrected report did not correspond to the desired Z_{max} report. There is a nearly linear relationship between average report error and range, with corrected estimates improving from an average report error of approximately 0.25 levels at close range to 0.15 levels at long range. The successful results of the U.S. threshold adjustment curve favor its selection over the current set of threshold adjustments for use in compensating ASR–9 beam filling losses.

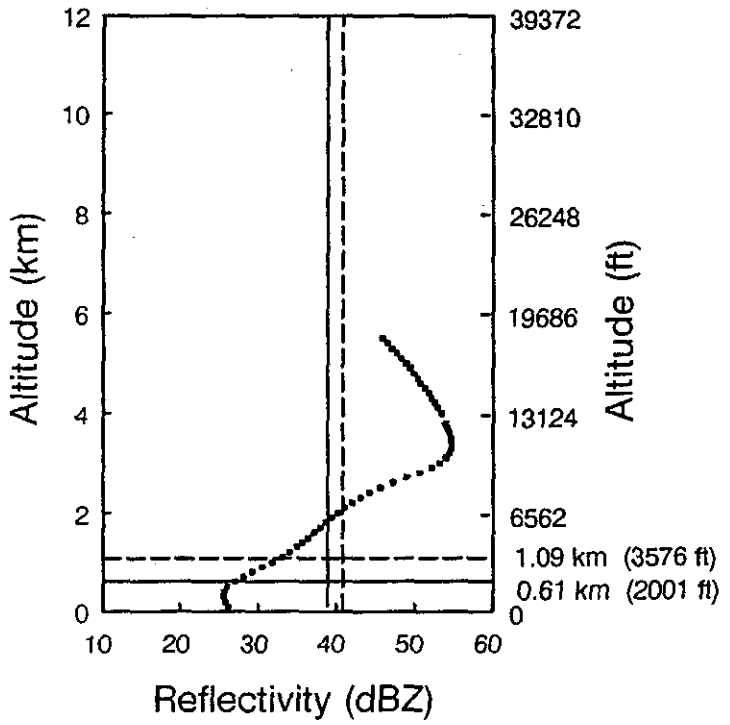

Figure 24. Example reflectivity profile where Z_{max} is at least two weather levels greater than the corrected Z_{asr} (low beam Z_{asr} is shown with solid vertical line, high beam Z_{asr} is shown with dashed vertical line). Altitude extents of the upper 3 dB edge of the high and low beam are indicated with dashed and solid horizontal lines respectively. The profile is from Denver taken on 9/5/87 at approximately 23:20 UTC and was located at 61° azimuth, 4.3 nmi range.

Reflectivity levels of thunderstorm anvils are especially difficult for the ASR-9 to accurately estimate. These anvils consist of a thin layer (usually less than 10,000 ft) of ice-crystals which have been sheared off by strong upper-level winds near the tops of thunderstorms and may extend several kilometers downwind. Due to the low particle densities and ice crystal composition of these anvils, they are weakly reflective, seldom exceeding 25 dBZ (level 1). Although the limited altitude extent of these high altitude features results in as much as 20 dBZ underestimation of the actual reflectivity by the ASR-9, the thunderstorm anvils are usually correctly reported as level 1 (recall that the level 1 threshold is tied to the system noise level, so that any detection at all counts as a level 1 detection).

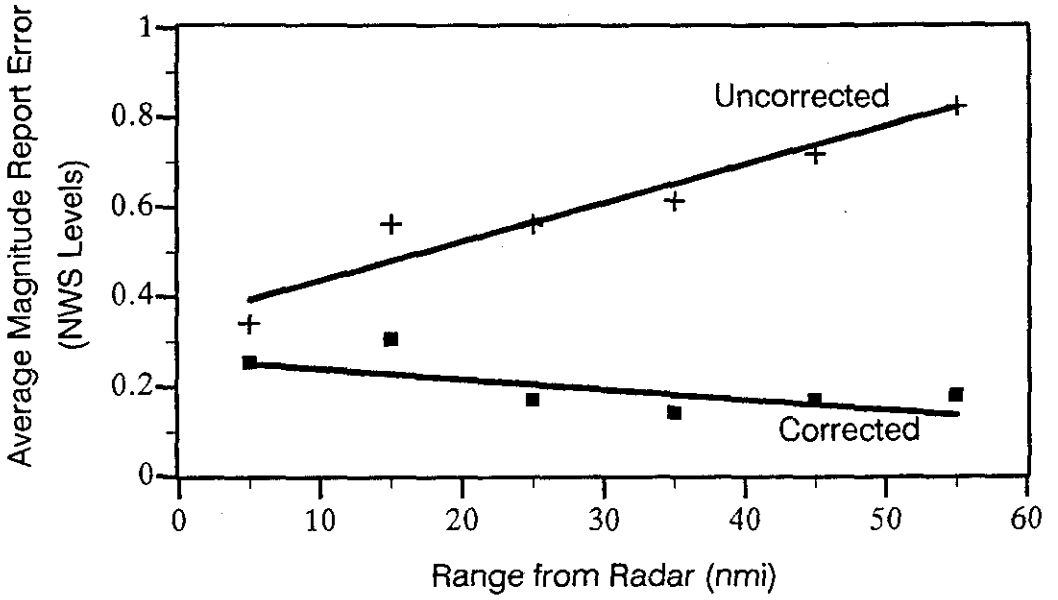

Figure 23. Average weather report error versus profile range from radar for the entire test data set. Errors without any correction (upper line, plusses) clearly exceed errors after correction (lower line, filled squares).

Table 3.
Results of the U.S. Correction on the Test Data Set, with All Sites and Ranges Taken as a Whole.

Success of Correction	% of Profiles	% Severe
correct estimate	79.9	22.6
error of 1 level	18.6	32.2
error of 2 or more levels	1.6	69.4

A profile which is typical of those for which corresponding corrected weather reflectivity reports underestimated the Z_{max} level by two or more levels is shown in Figure 24. This profile was located at 62° azimuth, 4.3 nmi range, and was located in close proximity (less than 1 nmi away) to an intense thunderstorm cell with maximum reflectivity greater than 55 dBZ. A vertical cross-section through this storm indicates a broadening of the storm cell with height. Because of this, the vertical profile exhibits a sharp increase in reflectivity corresponding to interception of the overhanging precipitation associated with the storm. The profile maximum occurs at about 3.5 km — more than 2 km above the upper 3 dB edge of the high beam. Thus, at this close range, the ASR-9 beams are relatively insensitive to the elevated reflectivity peak and a resultant underestimation of over 12.5 dBZ (2 NWS levels) occurs.

4. SUMMARY AND CONCLUSIONS

This report documents computation of a set of reflectivity threshold adjustments for the ASR–9 reflectivity channel. The computational method is based on knowledge of the relationship between storm reflectivity structures and their representation by the six–level weather reflectivity channel of the ASR–9. Previous studies have shown that a fan–beam radar such as the ASR–9 may significantly underestimate the reflectivity of a storm if the precipitation non–uniformly or partially fills the vertically broad beam. Thus, the NWS weather level thresholds must be adjusted to provide accurate reports of storm intensity.

The ASR–9 reflectivity channel should produce a useful two–dimensional reflectivity representation for air traffic control purposes. The vertical profile maximum reflectivity projection Z_{max} was identified as a plausible representation in that it attempts to report those regions of most intense convective activity. It is conservative in that it indicates the worst conditions which may be encountered by an aircraft at any altitude.

Five regions across the continental U.S. were identified for this study. Volumetric pencil–beam radar data were collected from one site in each region and were used to construct vertical profiles of reflectivity. By using our ASR–9 weather channel simulation facility, we were able to calculate the reflectivity scaling factors (reciprocals of threshold adjustments) which minimized the error between Z_{asr} and Z_{max}. This computation was performed separately for each site and weather level combination. Similarities in the threshold adjustment curves suggested that a single U.S. correction might be appropriate for all sites and weather levels. The single U.S. threshold adjustment curve computed was found to lie within one standard deviation of nearly all of the site/level specific correction curves.

The ASR–9 weather report accuracy relative to Z_{max} was assessed for reports which were uncorrected, corrected using the current threshold adjustments, and corrected using the single U.S. threshold adjustments. The U.S. threshold adjustments were found to significantly improve ASR–9 weather reflectivity report accuracy for producing the maximum profile reflectivity. Approximately 80 percent of the profiles were correctly assigned the NWS weather level corresponding to Z_{max}, and 98 percent of the profiles were adjusted to within one level of Z_{max}.

The single U.S. reflectivity threshold adjustments proposed for the ASR–9 produce significantly improved reports of maximum storm intensity over the currently implemented adjustments. Variations in storm structure among sites and weather intensities were not found to be significant for the Z_{max} representation. This report has documented an appropriate method for computing threshold adjustments for the ASR–9 reflectivity channel. This method was used to determine weather reflectivity threshold adjustments which will allow the ASR–9 to produce conservative reports of storm intensity.

Lincoln Laboratory has stationed observers in the Orlando International Airport TRACON during summertime operational testing of the Terminal Doppler Weather Radar (TDWR) and ASR Wind Shear Processor (ASR–WSP) in 1990 and 1991. Since the Orlando TRACON has an operational ASR–9, the observations gathered will provide further insight into controller perception and interpretation of the current six–level weather presentation, thus allowing us to further assess the appropriateness of the vertical reflectivity maximum report for air traffic control purposes.

GLOSSARY OF SYMBOLS

B_t	Relative power of transmit beam
B_r	Relative power of receive beam
H	Height
M	Number of reflectivity values averaged together to determine Z_{max}
N	Number of profiles in an ensemble
R	Range
Z	Reflectivity factor
Z_{asr}	Equivalent ASR–9 reflectivity factor
Z_{avg}	Linear average of reflectivities of a vertical profile
Z_{max}	Maximum reflectivity of a vertical profile
Z_{sfc}	Near–surface reflectivity of a vertical profile
Z_{six}	Reflectivity quantized into the six NWS weather levels
ϵ	Mean square error between Z_{max} and Z_{asr}
η	Reflectivity scaling factor that minimizes ϵ
θ	Azimuth angle
ϕ	Elevation angle

REFERENCES

M.A. Alaka, R.C. Elvander, and R.E. Saffle, "Nowcasts and short-range (0-2 hour) forecasts of thunderstorms and severe convective weather for use in air traffic control," Technical Report, U.S. Dept. of Commerce, NOAA, FAA-RD-79-98 (1979).

E.B. Dobson, A. Arnold, and F.L. Robison, "Weather detection using fan-beam radars," *Preprints, 18th Conference on Radar Meteorology*, American Meteorological Society, Atlanta, GA, 1978, 413-416.

R.J. Donaldson, "Radar reflectivity profiles in thunderstorms," *J. Meteor.*, 18, 292-305 (1961).

D.R. Easterling and P.J. Robinson, "The diurnal variation of thunderstorm activity in the United States," *J. Climate Appl. Meteor.*, 24, 1048-1058 (1985).

D.R. Greene, "A comparison of echo predictability: constant elevation vs. VIL radar data patterns," *Preprints, 15th Radar Meteorology Conference*, American Meteorological Society, Champaign-Urbana, IL, 1972, 111-116.

O. Hertzman and P.V. Hobbs, "The mesoscale and microscale structure and organization of clouds and precipitation in midlatitude cyclones. part XIV: three-dimensional airflow and vorticity budget of rainbands in a warm occlusion," *J. Atm. Sciences*, 45, 893-914 (1988).

J. Joss and A. Waldvogel, "Precipitation estimates and vertical reflectivity profile corrections," *Preprints, 24th Conference on Radar Meteorology*, American Meteorological Society, Tallahassee, FL, 1989, 682-688.

T.G Konrad, "Statistical models of summer rainshowers derived from fine-scale radar observations," *J. Appl. Meteor.*, 17, 171-188 (1978).

D.C. Puzzo, S.W. Troxel, M.A. Meister, M.E. Weber, J.V. Pieronek, "ASR-9 weather channel test report," MIT Lincoln Laboratory, Lexington, Mass., Project Report ATC-165, 1989, FAA-PS-89-3.

M.E. Weber, "Assessment of ASR-9 weather channel performance: analysis and simulation," MIT Lincoln Laboratory, Lexington, Mass., Project Report ATC-138, 1986, FAA-PM-86-16.

H.D. Young, *Statistical Treatment of Experimental Data*, New York: McGraw-Hill (1962).

APPENDIX A

VOLUME SCAN DATA USED FOR DETERMINING BEAM FILLING LOSS ADJUSTMENTS

The data used in this study were chosen to provide vertical reflectivity profiles for a variety of storm types and intensities in five geographic locations. Although not specifically used in the analysis, each volume scan was assigned an intensity category based on the most developed cell in the scan. Three intensity categories were defined and used: weak, moderate, and strong. Specific criteria for the categorization are given in Table A–1. The cloud top height was defined as the greatest height of the 18 dBZ contour, and the core reflectivity was the reflectivity of the innermost region of the most intense storm cell in the volume scan. A complete list of volume scans for each site is given in Tables A–2 through A–7.

Table A–1.
Storm Intensity Classification Scheme.

Category	Description
Weak	Core reflectivity < 41 dBZ (NWS Levels 1 and 2). Cloud tops < 25,000 feet.
Moderate	Core reflectivity between 41 and 50 dBZ (NWS Levels 3 and 4). Cloud tops between 25,000 and 35,000 feet.
Strong	Core reflectivity > 50 dBZ (NWS Levels 5 and 6). Cloud tops > 35,000 feet.

Table A-3.
Volume Sfcans from Denver Taken by Lincoln Laboratory C-band Radar

Type	Date	Time	Storm Intensity	Number of Tilts	Maximum Elev. Angle
airmass	5/18/87	20:59:47	moderate	12	40
airmass	5/18/87	21:15:13	moderate	12	40
airmass	5/18/87	21:33:08	moderate	12	40
airmass	5/18/87	21:46:26	moderate	12	40
airmass	5/18/87	21:59:45	weak	12	40
airmass	5/18/87	22:30:37	strong	16	20
airmass	5/21/88	21:24:07	weak	17	40
airmass	5/21/88	21:37:54	weak	17	40
airmass	5/21/88	22:08:47	weak	17	40
airmass	5/21/88	22:19:03	weak	17	40
airmass	6/08/87	21:41:04	moderate	10	12
airmass	6/08/87	21:51:03	moderate	10	10
airmass	6/08/87	22:00:09	moderate	6	12
airmass	6/08/87	22:09:21	moderate	7	12
airmass	6/08/87	22:32:01	weak	7	12
airmass	7/07/87	01:10:11	moderate	8	12
airmass	7/07/87	01:23:00	moderate	8	13
airmass	7/07/87	01:39:48	moderate	8	16
airmass	7/07/87	01:47:44	moderate	12	35
airmass	7/07/87	02:01:16	moderate	9	13
airmass	7/07/87	02:06:19	moderate	9	13
airmass	7/07/87	02:11:21	moderate	9	13
airmass	7/07/87	02:16:23	moderate	9	13
airmass	7/07/87	02:22:34	moderate	8	16
airmass	7/11/87	22:23:08	weak	9	13
airmass	7/11/87	22:38:03	moderate	9	13
airmass	7/11/87	22:59:30	weak	13	35
severe	6/18/87	22:25:19	strong	13	40
severe	6/18/87	22:35:14	strong	13	40
severe	7/03/87	02:50:05	strong	13	35

Table A–2.
Volume Scans from Boston Taken by MIT S–band Radar.

Type	Date	Time	Storm Intensity	Number of Tilts	Maximum Elev. Angle
airmass	5/03/83	10:13:00	moderate	10	20
airmass	5/03/83	10:33:00	moderate	10	20
airmass	5/03/83	10:53:00	moderate	10	20
airmass	5/03/83	11:13:00	moderate	10	20
airmass	5/03/83	11:33:00	moderate	10	20
airmass	6/13/85	13:30:00	moderate	9	15
airmass	6/13/85	15:01:00	moderate	9	15
airmass	6/20/85	17:59:00	moderate	9	15
airmass	6/20/85	20:06:00	weak	9	15
frontal	2/28/84	10:35:00	moderate	9	15
frontal	2/28/84	16:34:00	moderate	9	15
frontal	3/28/84	19:30:00	weak	9	15
frontal	3/28/84	23:42:00	weak	9	15
severe	5/20/82	13:39:00	strong	9	15
severe	5/20/82	13:59:00	strong	9	15
severe	5/20/82	14:35:00	strong	9	15
severe	5/20/82	14:47:00	strong	9	15
severe	6/16/82	13:09:00	moderate	9	15
severe	6/16/82	13:31:00	moderate	10	20
severe	6/16/82	14:20:00	moderate	10	20
severe	6/16/82	15:46:00	moderate	9	15
severe	6/16/82	16:46:00	moderate	9	15
severe	6/16/82	19:43:00	moderate	9	15
stratiform	3/13/84	15:42:00	weak	9	15
stratiform	3/13/84	17:30:00	weak	9	15
stratiform	3/13/84	21:15:00	weak	9	15
stratiform	4/08/85	19:36:00	weak	5	3
stratiform	4/08/85	20:16:00	weak	5	3
stratiform	4/18/85	20:55:00	weak	7	5
stratiform	4/18/85	22:35:00	weak	7	5

Table A–4.
Volume Scans from Huntsville Taken by MIT C-band Radar.

Type	Date	Time	Storm Intensity	Number of Tilts	Maximum Elev. Angle
airmass	3/31/88	20:15:27	moderate	6	8
airmass	3/31/88	21:17:01	strong	10	24
airmass	3/31/88	21:23:19	strong	10	24
airmass	3/31/88	21:27:11	moderate	10	24
airmass	6/02/88	19:39:30	moderate	18	24
airmass	6/02/88	19:43:05	moderate	18	24
airmass	7/14/88	17:54:45	strong	10	13
airmass	7/14/88	18:40:43	strong	18	26
airmass	7/14/88	19:46:26	strong	9	11
airmass	7/14/88	20:01:30	strong	13	17
airmass	7/14/88	20:35:42	strong	14	18
airmass	7/14/88	21:47:20	moderate	20	27
airmass	7/14/88	22:54:24	strong	12	16
airmass	7/15/88	03:22:42	strong	9	11
airmass	7/15/88	03:53:39	strong	16	21
airmass	7/16/88	21:18:33	strong	12	16
airmass	8/11/88	22:22:49	strong	10	13
airmass	8/11/88	22:28:50	strong	9	11
airmass	8/11/88	22:42:09	moderate	15	37
severe	5/10/88	00:35:15	moderate	9	12
severe	5/10/88	00:39:28	strong	9	12
severe	5/10/88	00:45:50	strong	7	9
severe	5/10/88	00:50:16	moderate	10	13
severe	5/23/88	04:11:29	moderate	8	11
severe	5/23/88	04:15:12	moderate	7	9
severe	5/23/88	04:20:34	moderate	8	11
severe	9/24/88	18:40:33	strong	7	9
severe	9/24/88	18:44:32	strong	9	11
severe	9/24/88	18:49:29	strong	7	9
severe	9/24/88	18:56:49	moderate	10	13

Table A-3 (Continued).
Volume Scans from Denver Taken by *Lincoln Laboratory* C-band Radar.

Type	Date	Time	Storm Intensity	Number of Tilts	Maximum Elev. Angle
severe	7/03/87	02:56:49	strong	13	35
severe	7/03/87	03:03:54	strong	13	35
severe	9/05/87	22:48:27	moderate	12	35
severe	9/05/87	23:05:01	strong	12	35
severe	9/05/87	23:18:51	strong	12	35
severe	9/05/87	23:34:06	strong	12	35
severe	9/05/87	23:39:09	strong	12	35
stratiform	7/12/87	00:58:15	weak	8	12
stratiform	7/12/87	01:04:39	weak	8	12
stratiform	7/12/87	01:07:51	weak	8	12
stratiform	8/21/87	22:55:41	weak	12	35
stratiform	8/21/87	23:05:48	weak	12	35
stratiform	8/21/87	23:15:13	weak	12	35
stratiform	8/21/87	23:25:18	weak	12	35
stratiform	8/21/87	23:32:19	weak	10	15
stratiform	8/21/87	23:44:28	weak	10	15
stratiform	11/15/87	18:38:42	weak	10	12
stratiform	11/15/87	18:58:39	weak	10	12

Table A–5.
Volume Scans from Kansas City Taken by Lincoln Laboratory C–band Radar.

Type	Date	Time	Storm Intensity	Number of Tilts	Maximum Elev. Angle
airmass	5/14/89	18:10:51	moderate	18	40
airmass	5/14/89	18:20:51	moderate	16	40
airmass	5/14/89	18:23:53	moderate	15	40
airmass	5/14/89	18:29:59	weak	14	18
airmass	5/14/89	18:38:25	weak	16	40
airmass	5/14/89	18:44:28	weak	16	40
airmass	5/14/89	18:50:32	weak	16	40
airmass	6/07/89	21:17:41	moderate	9	30
airmass	6/07/89	21:21:17	moderate	11	29
airmass	6/07/89	21:29:51	moderate	16	40
airmass	6/07/89	21:32:53	moderate	15	40
airmass	6/07/89	21:35:57	moderate	16	40
airmass	6/07/89	21:38:58	moderate	15	40
airmass	6/07/89	21:41:59	moderate	16	40
airmass	6/07/89	21:45:01	moderate	15	40
airmass	7/01/89	21:56:23	moderate	12	40
airmass	7/01/89	22:03:18	moderate	18	40
airmass	7/01/89	22:13:19	moderate	18	40
airmass	7/01/89	22:23:20	moderate	18	40
airmass	7/01/89	22:33:23	moderate	18	40
frontal	6/01/89	00:48:21	weak	9	12
frontal	6/01/89	00:53:51	weak	9	12
frontal	6/01/89	00:59:20	weak	9	12
frontal	6/01/89	01:04:50	weak	9	12
frontal	6/01/89	01:10:19	weak	9	12
frontal	6/01/89	01:15:48	weak	9	12
frontal	6/18/89	02:30:17	strong	15	40
frontal	6/18/89	02:36:21	strong	15	40
frontal	6/18/89	02:42:23	strong	15	40
frontal	6/18/89	02:48:23	strong	15	40

Table A–4 (Continued).
Volume Scans from Huntsville Taken by MIT C–band Radar.

Type	Date	Time	Storm Intensity	Number of Tilts	Maximum Elev. Angle
stratiform	1/19/88	21:43:11	weak	8	11
stratiform	1/19/88	21:49:34	weak	8	11
stratiform	2/02/88	17:10:35	weak	8	11
stratiform	2/11/88	17:34:56	weak	8	11
stratiform	9/11/88	22:08:52	moderate	6	7
stratiform	9/11/88	22:15:09	moderate	9	11
stratiform	9/11/88	22:26:47	weak	7	9
stratiform	9/11/88	22:36:48	weak	7	9
stratiform	9/11/88	22:40:59	weak	10	13
stratiform	9/29/88	15:01:33	weak	7	9
stratiform	9/29/88	15:06:38	weak	12	16
stratiform	9/29/88	15:11:15	weak	7	9
stratiform	10/18/88	22:12:03	moderate	13	17
stratiform	10/18/88	22:57:19	moderate	13	27
stratiform	10/18/88	23:14:58	moderate	15	24
stratiform	10/18/88	23:20:20	weak	13	22
stratiform	10/20/88	16:19:14	weak	9	11
stratiform	10/20/88	20:08:36	weak	9	11
stratiform	10/20/88	21:22:15	weak	9	11
stratiform	10/20/88	22:01:40	weak	8	10
stratiform	10/28/88	10:03:51	weak	12	16
stratiform	10/28/88	10:08:40	weak	11	14
stratiform	10/28/88	10:13:03	weak	10	13
stratiform	10/31/88	14:33:12	weak	8	10
stratiform	10/31/88	14:40:41	weak	8	10
stratiform	10/31/88	15:36:26	weak	9	11

Table A–5 (Continued).
Volume Scans from Kansas City Taken by Lincoln Laboratory C–band Radar.

Type	Date	Time	Storm Conditions	Number of Tilts	Maximum Elev. Angle
stratiform	4/20/89	18:18:59	weak	10	16
stratiform	4/23/89	19:26:38	weak	16	40
stratiform	4/23/89	19:31:17	weak	18	40
stratiform	4/23/89	19:36:21	weak	18	40
stratiform	4/23/89	19:41:21	weak	18	40
stratiform	4/23/89	19:46:20	weak	18	40
stratiform	4/23/89	19:51:21	weak	18	40
stratiform	4/23/89	19:56:20	weak	18	40
stratiform	4/10/89	22:38:16	weak	9	12
stratiform	6/10/89	22:49:29	weak	9	12
stratiform	6/10/89	23:00:42	weak	9	12

Table A-5 (Continued). Volume Scans from Kansas City Taken by Lincoln Laboratory C-band Radar.

Type	Date	Time	Storm Intensity	Number of Tilts	Maximum Elev. Angle
frontal	6/18/89	02:54:27	strong	15	40
severe	5/08/89	22:25:59	strong	14	18
severe	5/08/89	22:30:56	strong	14	18
severe	5/08/89	22:35:51	strong	13	16
severe	5/08/89	22:39:18	strong	14	18
severe	5/08/89	22:43:19	strong	14	18
severe	5/08/89	22:47:21	strong	14	18
severe	5/08/89	22:51:22	strong	14	18
severe	5/08/89	22:59:25	strong	14	18
severe	5/25/89	01:41:22	strong	13	40
severe	5/25/89	01:53:21	strong	18	40
severe	5/25/89	02:01:24	strong	15	40
severe	5/25/89	02:07:27	strong	15	40
severe	5/25/89	02:13:31	strong	15	40
severe	5/25/89	02:19:35	strong	15	40
stratiform	4/02/89	19:26:31	moderate	17	40
stratiform	4/02/89	19:31:29	moderate	17	40
stratiform	4/02/89	19:36:25	weak	17	40
stratiform	4/02/89	19:41:22	weak	17	40
stratiform	4/02/89	19:46:19	weak	17	40
stratiform	4/02/89	19:51:17	weak	17	40
stratiform	4/02/89	19:56:14	weak	17	40
stratiform	4/20/89	17:53:12	weak	14	18
stratiform	4/20/89	17:57:12	weak	14	18
stratiform	4/20/89	18:01:13	weak	11	21
stratiform	4/20/89	18:04:11	weak	11	21
stratiform	4/20/89	18:07:08	weak	11	21
stratiform	4/20/89	18:10:06	weak	11	21
stratiform	4/20/89	18:13:04	weak	11	21
stratiform	4/20/89	18:16:01	weak	11	21

Table A–7.
Volume Scans from Seattle Taken by NCAR CP–3 Radar.

Type	Date	Time	Storm Intensity	Number of Tilts	Maximum Elev. Angle
stratiform	2/13/82	00:44:10	weak	12	15
stratiform	2/13/82	04:30:15	weak	11	15
stratiform	2/13/82	04:55:14	weak	11	15
stratiform	2/13/82	05:20:15	weak	11	15
stratiform	2/13/82	06:09:14	weak	11	15
stratiform	2/13/82	06:42:18	weak	11	15
stratiform	2/13/82	07:07:15	weak	11	15
stratiform	2/13/82	07:58:15	weak	11	15
stratiform	2/13/82	11:06:04	weak	11	19
stratiform	2/13/82	11:39:15	weak	12	15
stratiform	2/13/82	12:24:04	weak	11	19
stratiform	2/13/82	12:55:15	weak	11	15
stratiform	2/13/82	13:39:04	weak	11	19
stratiform	2/13/82	14:16:14	weak	11	15
stratiform	2/13/82	15:00:04	weak	11	19
stratiform	2/13/82	15:25:15	weak	11	15
stratiform	2/13/82	15:49:15	weak	12	15
stratiform	2/13/82	16:14:44	weak	11	15
stratiform	2/13/82	16:39:15	weak	11	15
stratiform	2/13/82	17:30:15	weak	11	15
stratiform	2/13/82	18:59:21	weak	11	15
stratiform	2/13/82	19:23:36	weak	11	15
stratiform	2/13/82	20:53:45	weak	11	15
stratiform	2/13/82	21:18:15	weak	11	15
stratiform	2/13/82	21:54:25	weak	11	15
stratiform	2/13/82	22:33:44	weak	11	15
stratiform	2/13/82	23:02:15	weak	11	15
stratiform	2/13/82	23:27:15	weak	11	15
stratiform	2/13/82	23:51:15	weak	11	15
stratiform	2/14/82	00:16:15	weak	11	15
stratiform	2/14/82	02:35:15	weak	11	15

Table A–6.
Volume Scans from Seattle Taken by NCAR CP–4 Radar.

Type	Date	Time	Storm Intensity	Number of Tilts	Maximum Elev. Angle
stratiform	1/16/82	18:02:42	weak	10	15
stratiform	1/16/82	19:54:07	weak	11	15
stratiform	1/16/82	21:38:17	weak	11	15
stratiform	1/16/82	22:45:59	weak	11	15
stratiform	1/16/82	23:19;50	weak	11	15
stratiform	1/16/82	23:41:16	weak	11	15
stratiform	1/17/82	06:54:04	weak	13	12
stratiform	1/22/82	11:23:32	weak	10	9
stratiform	1/22/82	12:31:26	weak	11	15
stratiform	1/22/82	14:00:51	weak	9	7
stratiform	1/22/82	15:31:08	weak	9	7
stratiform	1/22/82	16:50:20	weak	9	9
stratiform	1/22/82	18:17:51	weak	9	7
stratiform	1/22/82	20:10:20	weak	9	9
stratiform	1/22/82	21:54:20	weak	9	9
stratiform	1/22/82	22:48:20	weak	9	9
stratiform	1/23/82	00:08:21	weak	9	9
stratiform	1/23/82	01:33:14	weak	9	9
stratiform	1/23/82	02:45:21	weak	9	7
stratiform	1/23/82	06:58:02	weak	10	9
stratiform	1/23/82	09:16:54	weak	11	15
stratiform	1/23/82	10:41:57	weak	11	15
stratiform	1/23/82	12:12:00	weak	11	15
stratiform	1/23/82	13:37:32	weak	11	15
stratiform	1/23/82	15:01:33	weak	11	15
stratiform	1/23/82	16:27:05	weak	11	15
stratiform	1/23/82	17:52:38	weak	11	15
stratiform	1/24/82	04:41:20	weak	11	19
stratiform	1/24/82	06:19:20	weak	11	19

Table A-7 (Continued).
Volume Scans from Seattle Taken by NCAR CP-3 Radar.

Type	Date	Time	Storm Intensity	Number of Tilts	Maximum Elev. Angle
stratiform	2/14/82	02:53:28	weak	11	19
stratiform	2/14/82	04:19:15	weak	11	15
stratiform	2/14/82	05:10:15	weak	11	15
stratiform	2/14/82	06:01:15	weak	11	15
stratiform	2/14/82	06:19:28	weak	11	19
stratiform	2/14/82	06:52:15	weak	11	15
stratiform	2/14/82	07:43:15	weak	11	15